2015

Sub-Marine Sediment Instability near Southwest Pass of the Mississippi River: Evidence of Mass Movements from Raciochemistry and Other Proxies

Gregory Paul Keller
Louisiana State University and Agricultural and Mechanical College

SUB-MARINE SEDIMENT INSABILITY NEAR SOUTHWEST PASS OF THE MISSISSIPPI RIVER: EVIDENCE OF MASS MOVEMENTS FROM RADIOCHEMISTRY AND OTHER PROXIES

A Thesis

Submitted to the Graduate Faculty of the
Louisiana State University and
Agricultural and Mechanical College
in partial fulfillment of the
requirements for the degree of
Master of Science

In

The Department of Geology and Geophysics

by
Gregory P. Keller
B.S., Louisiana State University and Agricultural and Mechanical College, 2013
December 2015

Acknowledgments

I would like to thank the Bureau of Ocean Energy Management for the funding for this project. I would also like to thank the LSU Dept. of Geology and Geophysics, New Orleans Geologic Society, and The Devon Energy Corporation for additional funding.

A special thanks to Sam Bentley, for great advising on field work, lab work, writing, potential for employment, how to smoke a pig, homebrewing, and an entertaining, never-ceasing commentary on the Louisiana country-side on our numerous commutes to field work. Thanks to Kevin Xu and Karen Luttrell for serving on my committee, and Ioannis Georgiou and Mike Miner for input on my presentations at BOEM project meetings.

I would like to thank Jillian Maloney for help with field work, brainstorming, help with figures, and her hard work on the MRDF project. Thanks to Jeff Obelcz for help with fieldwork our countless brainstorming sessions. Crawford, you helped with too many things to list, but thanks buddy! Thanks to Ryan, Brianna and Suyapa for assistance with grain size!! Thanks to Bryan, Evan, Franky, James, Pat, Ray, Roddy, and Ross for everything you guys have done around the lab like changing my samples and helping split cores. A special thanks to Jillian Maloney, Jeff Obelcz, and Meg O'Connor who have helped me with my favorite thing (editing) on abstracts, figure captions, and this thesis. Thanks to Carlo, Chris, Ethan, Jeff B., Jillian B., Kathryn, and Laura for being great lab mates!

Lastly, I have to thank my friends and family. Y'all have been so encouraging! A special shoutout to those at The Ring Community Church for asking 'what a geologist does,' and not tuning out when I explain to you why mud is so important! Y'all are great!

Table of Contents

List of Tables

List of Figures

List of Abbreviations

Disintegrations per minute per square cm (dpm/cm^2)

Disintegrations per minute per gram (dpm/g)

Gully (gul)

Lobe (lob)

Mississippi River (MR)

Mississippi River Delta Front (MRDF)

Prodelta (pro)

Sediment accumulation rate (SAR)

Southwest Pass (SW pass)

Undisturbed (und)

Abstract

Mass wasting events are an important geomorphic control on the Mississippi River Delta Front. Short multicores (<50 cm) and longer gravity cores (up to 3 m) were collected seaward of the Southwest Pass of the Mississippi River Delta and were analyzed to assess the frequency, extent, and potential causes of submarine mass wasting events. Cores were analyzed for radionuclide activity, grain size, and density at 2 cm resolution, with x-radiography for the whole core. Short-term sedimentation rates calculated from ^{7}Be are 2-16 cm/y, while longer-term accumulation from ^{210}Pb are only 1.3-7.3 cm/y.

In most cores, ^{210}Pb activity steadily decreases downcore without displaying a "stairstep" nature. However, seven cores have layers of low ^{210}Pb activity stratigraphically above layers with higher activity. In a gravity core from a mudflow gully, ^{210}Pb steadily decreases for the upper 70 cm before stabilizing for the remaining 150 cm. Clay content generally ranges between 25-40% and sand ranges between 5-15% with silt making up the rest of each sample. Sediment accumulation rates derived from ^{210}Pb in the short cores indicate that proximity to the river mouth has stronger influence than depositional environment (mudflow gully, depositional lobe, prodelta).

This finding may be explained by rapid sedimentation rates coupled with a reduced tropical cyclone activity over the delta in the last seven years (2006-2013) which is a known cause of mass wasting events. The regions of decreased ^{210}Pb activity may be evidence of scavenging effects of plume sedimentation because they do not correspond with decreases in clay fraction. The layer of homogenized activity below 70cm in the gully core corresponds with a layer of decreased density. This layer occurs at a depth equivalent to 9-18 years, indicating

mixing on a decadal scale from mudflows. These results may be explained by a lack of recent mass failures corresponding with lulls in tropical cyclone activity over the delta, preceded by a period of more active hurricane-driven mudflow activity.

1 Introduction

Muddy clinothems on continental shelves are commonly built with sediment delivered from a fluvial source, shaped by cross-shelf gradients in sediment accumulation (e.g., Slingerland et al., 2008). The morphology of such deltaic deposits is further influenced by dispersal processes including but not limited to waves, tides, and fluvial flows (Wright and Coleman, 1973; Galloway, 1975; Walsh and Nittrouer, 2009). The Mississippi River Delta has long been considered a river-dominated end member of deltaic morphology (Wright and Coleman, 1973; Walsh and Nittrouer, 2009), wherein major morphological features are produced by interacting river flows (delivering abundant sediment) and subsequent mass failures that remobilize and redistribute sediments (Coleman et al., 1980). These phenomena are characteristic of the Mississippi River Delta Front (Coleman et al., 1980), morphologically equivalent to the submarine foreset beds of the prograding Mississippi River delta and clinothem (Wright and Coleman, 1973).

The first major insights into submarine mass movements of the MRDF primarily were derived from comparison of bathymetric surveys, and early applications of sidescan sonar (Coleman et al., 1980). Coleman et al. (1980) and Prior and Suhayda (1979) described the motion of sediments in mudflow lobes, gullies, and other similar landforms as either slow, steady creeps or rapid movements that pulse over time, with downslope movement rates from hundreds of meters per year to up to 2 km per year. More recent work has evaluated regional dispersal patterns using radioisotope geochronology (Corbett et al., 2006; Young, 2014); in these studies, radiochemical tracers were used to study sedimentation rates and the annual input of sediment for movement by mass-movement events. These radiochemical studies have

focused mostly on regional-scale phenomena, covering wide regions of the Mississippi Delta continental shelf.

More recently, concerns regarding seafloor stability of the MRDF, and associated geohazards, and risk to petroleum production have focused interest on MRDF mass failures (Kaiser et al., 2009). Of particular interest are the range of temporal and spatial scales over which failures occur (Maloney et al., 2014; Obelcz et al., 2014), and the forcing mechanisms (Guidroz, 2009). In this study, we apply radioisotope geochronological methods (^{210}Pb, ^{137}Cs, and ^{7}Be) and other geological core analyses to evaluate sediment depositional and dispersal processes (including fluvial supply and mass failures) across the MRDF. This work is placed in context as part of a larger study of MRDF seabed evolution, which provides new geophysical and geological data to evaluate geological processes and products of the MRDF (Maloney et al., 2014).

2 Background

2.1 Study Area

The study area is the continental shelf proximal to the SW Pass distributary of the Mississippi River Delta, spanning water depths of 25 to 75 m (Figure 1). SW Pass is the

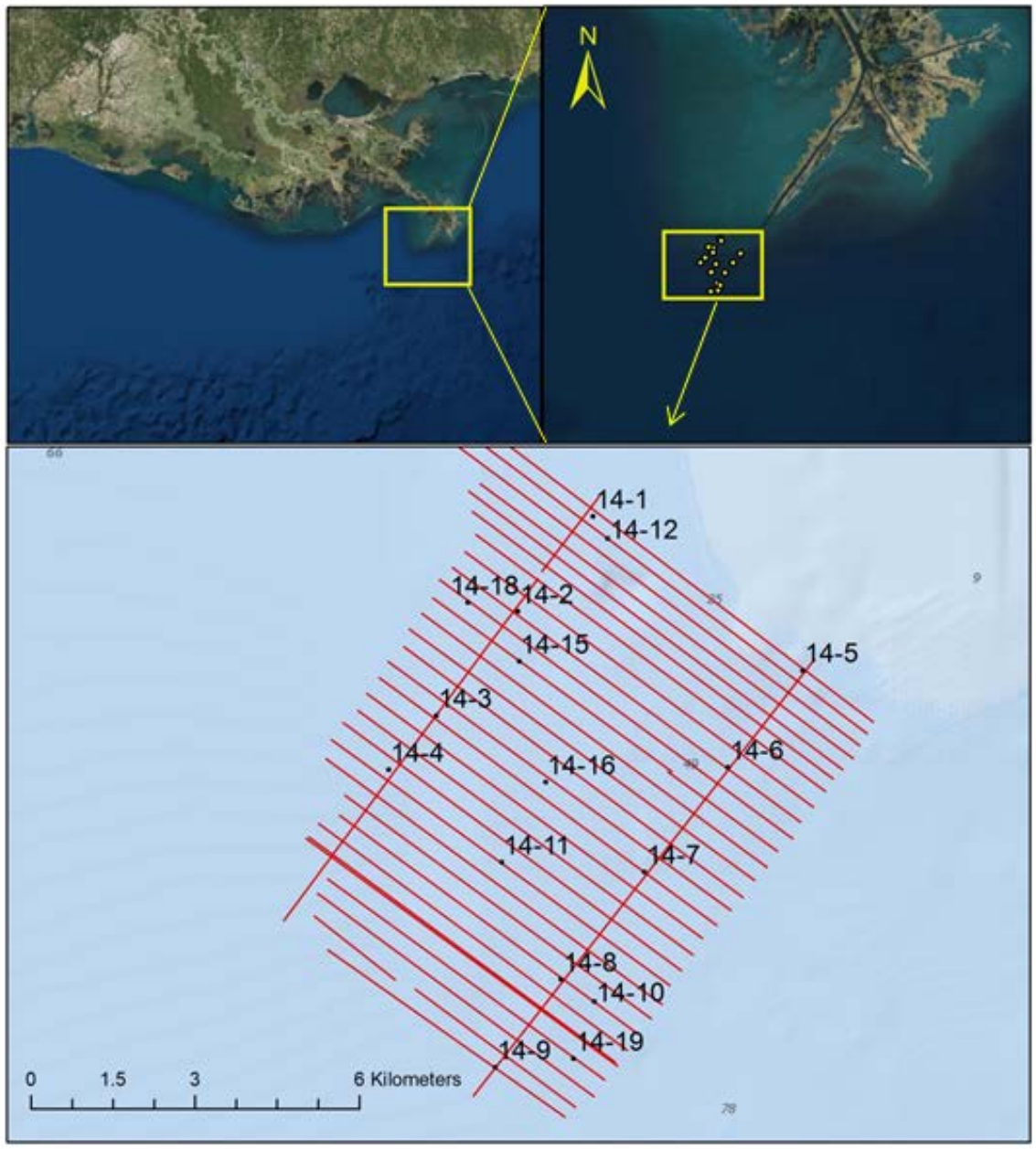

Figure 1: Map of study area. Coring locations are labeled with the core name; geophysical survey lines collected by Obelcz et al, 2014 are shown in red.

largest of three major distributary outlets of the modern Balize or Birdsfoot delta of the MR. The MR delivers approximately $2X10^8$ metric tons of suspended sediment to the northern Gulf of Mexico (GOM) shelf each year (Meade, 1996). For water years 2008-2010, SW Pass discharged ~$2X10^7$ metric tons of sediment per year, with the remainder of sediment exiting the river from other outlets (Allison et al., 2012). Much of the sediment is initially retained near the distributaries (within ~30km; Corbett et al, 2004; Xu et al. 2011), before being redistributed, with tropical cyclones being the most powerful forcing for sediment redistribution (Walsh et al., 2006). The four regions of the delta front based on bathymetry by Coleman et al. (1998) are interdistributary bay (0-10 m), upper delta front (10-70 m), intermediate delta front (70-120 m), and the lower delta front (120-200 m). Because much sediment dispersal is controlled by waves and currents interacting with the seabed, water depth is a controlling factor for where specific sediment transport processes occur (Coleman et al., 1980). Processes and phenomena leading to sediment-gravity flows on the shelf include rapid sedimentation, oversteepening of the seabed, and forces from long period waves present in hurricanes. Sediment mass transport stemming from these causes has a great effect on seabed morphology (Figure 2), which in turn affects the likelihood of further failures. Mass failure events pose a significant hazard to the vast array of drilling platforms and pipelines in the area (Sterling and Strohbeck, 1973; Guidroz, 2009; Kaiser et al., 2009).

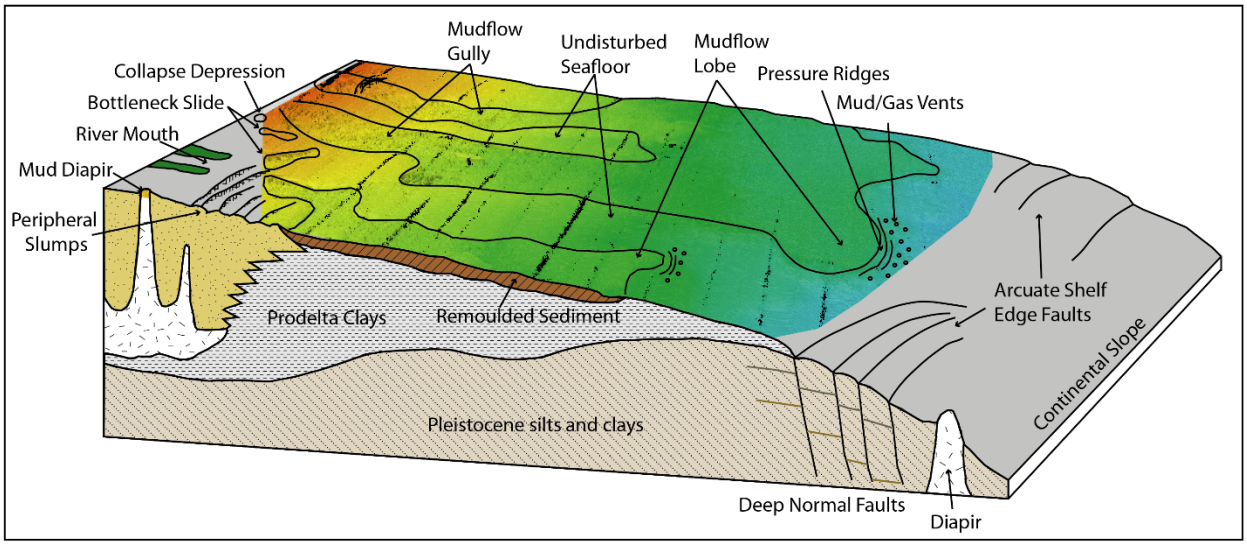

Figure 2: Seafloor diagram illustrating facies. Adapted from Coleman et al (1980) by Maloney et al (2014) using multi-beam bathymetry data from Walsh et al (2006). Outlined mudflow gullies cut into undisturbed seafloor and convey sediment downslope to depositional lobes which may stack and coalesce.

2.2 Types and Causes of Mass Failures

2.2.1 Sediment Transport Processes and Seabed Morphology

Figure 2 (from Maloney et al., 2014) illustrates major elements of MRDF seabed morphology, with terminology of Coleman et al. (1980) applied to a bathymetric surface from Walsh et al. (2006). Near SW Pass, collapse depressions and bottleneck slides occur primarily in interdistributary bays and the shallow upper delta front (0-70 m water depth). These features are relatively small (collapse depressions <150m wide; bottleneck slides <600m) and occur more frequently than larger features. Collapse depressions are bounded by curved escarpments up to 3m high. Bottleneck slides are bounded by scarps of similar scale; however, they are not completely enclosed. At the downslope end of bottleneck slides sediment is discharged and accumulates over the seafloor downslope (Figure 2).

Mudflow gullies are prevalent from interdistributary bays down through the intermediate delta front. Gullies are the most common features along the delta front. They have been observed in waters 6-90m deep (Coleman et al., 1980), and can incise up to 20m into the undisturbed seafloor. The gullies can be up to 10 km long, and join with other channels to form tributary systems. Slope failures are common along the edges of some of the larger channels, and source much of the material flowing through the structures. Mudflow lobes develop at downslope termini of gullies where sediment flowing through a feature with negative relief (gully) coalesces to form a depositional feature with positive relief (lobe; Figure 2; Coleman et al., 1980; Maloney et al., 2014).

Mudflow lobes are important depocenters at the end of gullies. They have an average thickness of 10 m, and coalesce and stack in a compensational manner analogous to sub-delta lobes and crevasse-splay deposits (Coleman et al., 1980; Maloney et al., 2014). No instantaneous rates of progradation have been measured, however they have been known to advance up to 900m downslope in one year, and can extend for 4 km. Failures in gullies have led to the transport and deposition of blocks up to 100 m in the some lobes.

2.2.2 Causes of Mass Failures

Mass failures develop where and when the downslope force of gravity acting on a mass of sediment exceeds resisting forces (Lee et al., 2009). Mass failures on the MRDF are facilitated by the low strength sea-floor sediments. Coleman et al. (1980) describe the formation of “weak plastic sediments” as being the result of rapid sedimentation (25 cm in a month, Coleman et al, 1980; 8 cm from the 2011 flood layer on the Atchafalaya shelf, Young, 2014; 16 cm from the 2014 flood layer near SW pass, this study) of low permeability silts and clays inhibiting pore

water flow. As the sediment is buried, the lack of dewatering increases pore pressure. Adding to the pore pressures is the generation of biogenic gasses (methane and carbon dioxide) from the degradation of organic matter deposited with the sediment. Obelcz et al. (2014) report the wide-spread presence of gas-charged sediments in this study's field area as detected by acoustic wipeout of sub-bottom sonar data. Denommee and Bentley (in press) also report gas charging on the SW Louisiana shelf, and seabed morphology produced by seabed failures similar to the MRDF. These unstable sediments can then be weakened further by cyclic loading associated with large waves (Coleman et al., 1980), especially those produced by major hurricanes crossing the Mississippi River Delta (Guidroz, 2009).

2.2.3 Hurricane Influence

Hurricanes are important triggers of mass movements offshore of the Mississippi River Delta. The associated long-period waves contribute to cyclic loading of the seabed, which can induce bottom shear stresses capable of causing failure (Coleman and Prior, 1978). Allison et al. (2005) observed a 20 cm event layer associated with two 2002 storms, Tropical Storm Isidore and Hurricane Lili. Mass movements associated with Hurricane Ivan destroyed seven platforms, and movements associated with Hurricane Katrina destroyed 46, with additional damage caused to infrastructure by both storms (Guidroz, 2009). Modeling efforts in the wake of Hurricane Ivan yield predicted maximum significant wave heights of 21 m (Wang et al., 2005) (compared to 17.9m observed), and associated bottom shear stresses strong enough to cause sediment failures at depths of up to 120m (Hooper and Suhayda, 2005). Since the record-breaking and very active hurricane seasons in 2004 and 2005, only three hurricanes have passed within 100 km of the study area with Gustav, a category 2 during its 2008 Louisiana

landfall, being the strongest of the three. Guidroz (2009) studied historical hurricane impacts on the MRDF seabed in detail, and ascertained that only category 3+ hurricanes that slowly traverse the MRDF are likely to produce seabed mass failures of scales sufficient to induce catastrophic platform collapse. Since the onset of Gulf of Mexico petroleum production, hurricanes in this category include Betsy (1965), Camille (1969), Ivan (2004), and Katrina (2005) (Guidroz, 2009).

2.3 Changes in the Modern System

As part of the broader Mississippi River source-to-sink sedimentary system (Bentley et al., 2015), the modern Balize delta lobe of the MR is being strongly influenced by upstream anthropogenic alterations such as dams, diversions, and bank stabilization that have reduced sediment load in the mainstem. Additional factors influencing delta land area and morphodynamics include local subsidence and eustatic sea-level rise; these influences are driving decreased sediment-transport efficiency that is accelerating in-channel sedimentation in the lower ~150 km of the river (Kemp et al., 2014), and upstream migration of major river discharge points. Allison et al. (2012) have shown that three outlets upstream of the Head of Passes (Fort St. Philip, Grand Pass, and Baptiste Collette) each currently discharge more suspended sediment than either South Pass or Pass a'Loutre. Collectively, these phenomena are likely to lead to backstepping of the Balize delta lobe (Bentley et al., 2015). Blum and Roberts (2009, 2012) present a long term decrease in the sediment load reaching the GOM, with as much as a 50% decline in the last century. One possible outcome of these changing sediment delivery patterns may be an overall decrease and subsequent redistribution of

sediment to different parts of the delta. This may increase failures in historically stable areas fed by distributaries that are capturing more sediment, or lead to fewer mass failures offshore of outlets experiencing declining sediment loads.

3 Methods

3.1 Field Work and Core Processing

Cores were collected offshore of SW Pass during the summer of 2014, from the *R/V Coastal Profiler* of the Louisiana State University's Coastal Studies Institute. Short (<50cm depth, 10 cm diameter) cores recovered from an Ocean Instruments MC-400 multi-corer and longer (up to 3m depth, 10 cm diameter) gravity cores were collected across four different facies (undisturbed seafloor, mudflow gully, depositional lobe, and prodelta). Facies were identified by the study of multi-beam bathymetry, sidescan, and subbottom seismic data collected from the *R/V Coastal Profiler* one week prior to coring (Obelcz et al., 2014). Coring sites selected to either coincide with subbottom seismic lines or locations previously cored by Young (2014), who used analytical methods similar to those of this study, but over a wider area with lower sampling density.

The multicore can recover four replicate cores per site. Of the four cores collected per deployment, one was extruded on deck into 2 cm sections for radiochemical and grain size analysis, one was subsampled for X-radiography by inserting a two-piece tray (2 cm thick) with sliding lid, to recover undisturbed sediment layers, and two were subsampled with thin-walled plastic tubes (7.5 cm diameter) to archive undisturbed sediments for future study.

Gravity cores were analyzed on a Geotek multi-sensor core logger for measurements of gamma density, magnetic susceptibility, and p-wave speed. Cores were subsequently split and sampled for grain size analysis, radiochemistry, and X-radiography (by extracting and archiving axial slabs 1.5 cm thick in clear acrylic plastic trays). All cores and subsamples were stored at 4°C until analysis.

3.2 Grain Size analysis

Sediment was subsampled from the multicore replicate that was extruded on deck or from the working half of the gravity cores after they were split. Small samples of wet sediment (< 1 ml) were placed into test tubes with 40mL of a 0.05% sodium phosphate solution to facilitate disaggregation, then dispersed in an ultrasonic bath to ensure particle dispersal (Huelse and Bentley, 2012). No acid or hydrogen peroxide was used to remove carbonate or organic matter. Data were then placed in volume-frequency-contour plots generated using Sigmaplot, to graphically show the percent abundance of all grain sizes between 0.38 and 2000 microns. A total of 515 sediment samples from 19 cores were analyzed for this study.

3.3 Radionuclide Analysis

Radionuclides of interest for the radiochemical analysis include ^{7}Be (natural cosmogenic, $t_{1/2}$=53.2 days), ^{210}Pb (natural ^{238}U-series, $t_{1/2}$=22.2 years), and ^{137}Cs (anthropogenic fallout, $t_{1/2}$=30.1 years). Samples for ^{7}Be measurement were analyzed within ~one half-life from the date of core collection. Water content was determined gravimetrically in samples for radionuclide analysis. Dried samples were then ground using a mortar and a pestle, then sealed into petri dishes. Samples for ^{7}Be analysis were performed immediately. Samples sat in the sealed dishes for 14 days before ^{210}Pb data were collected, to allow ingrowth of ^{210}Pb parent radionuclide ^{222}Rn, to determine supported activities. All samples were analyzed on Canberra LEGe or BEGe detectors, with samples from a single core being restricted to one detector. ^{210}Pb data were processed using the transmission method (Cochran et al., 2003). Activities associated with the 295 and 352 keV peaks of ^{214}Pb and the 609 keV peak of ^{214}Bi were averaged to determine the amount of supported ^{210}Pb. Supported ^{210}Pb activity is subtracted from total

^{210}Pb activity to determine excess Lead-210 ($^{210}Pb_{xs}$) activity. ^{7}Be inventories (disintegrations per minute per square cm, dpm/cm^2) were calculated by equation 1, from Muhammad et al. (2008):

$$I = \Sigma \rho_s \Delta z (1-\phi_i) A_i \qquad \text{Eq. 1}$$

where ρ_s is mineral density, Δz is thickness (cm) of the sample interval I (2 cm), ϕ_i is porosity (calculated by water loss at 60°C) and A_i is ^{7}Be activity (dpm/g). Sediment accumulation rates (SAR) were calculated using Sigmaplot© to perform least squares regressions on $^{210}Pb_{xs}$ data using the application of equation 2, from Muhammad et al (2008):

$$A_z = A_0 e^{(-\lambda z/S)} \qquad \text{Eq. 2}$$

where A_z is activity at depth z (dpm/g), A_0 is activity extrapolated to the sediment surface (dpm/g), λ is the decay constant of ^{210}Pb (y^{-1}), and S is the sediment accumulation rate (cm/y). A total of 503 sediment slices from 19 cores were analyzed for radionuclide activity.

3.4 X-Radiography

Sediments preserved in acrylic trays from multi-core deployments as well as slabs preserved in trays after gravity cores were split were used to generate X-radiograph images. X-radiographs were taken using a Thales Flashscan 35 digital X-ray detector illuminated by a Medison Acoma portable X-ray unit. A total of 48 images were collected as 14-bit grayscale TIFF files and refined for observation using Adobe Photoshop.

4 Results

4.1 Grain Size

Frequency-contour plots of grain size are shown in Figure 3. Grain size does not vary greatly in analyzed samples. Silt is the most dominant grain size in the field area, making up 40-60% of most samples by volume. Maximum and minimum silt values are 71 and 41%, respectively. The vast majority of samples have a modal grain size in the very fine or fine silt range (6-8 ϕ, 3.9-15.6 μm). Clay content ranges from 16 to 42%, with most samples containing 25-35%. Sand content ranges from 0 to 39% with most samples containing 5-15%. A small number of samples have higher sand content, including an 8 cm layer (36-44 cm) in gravity core 14-3g with 32-38% sand.

4.2 Gamma Density

Figure 4 displays gamma density profiles for cores 14-3g (depositional lobe), 14-6g (mudflow gully), and 14-9g (prodelta). Density profiles for the gravity cores show notable variation among the cores, as well as with depth in a single core. Cores 14-3g and 14-6g have 10-20 cm zones of relatively low density at core tops. The density at the surface of 14-3g is 2.02 g/cm^3. Much of the top section of the core (0-140 cm) varies slightly between values of 2.1 and 2.3 g/cm^3, with a local maximum at 38 cm of 2.45 g/cm^3, coincident with an increase in sand content described above. The lowest value of the core is 1.86 g/cm^3 at a depth of 66 cm, and it does not correspond with deviations in any other measured data. The bottom section of the core (140-292 cm) varies between 2.2 and 2.4 g/cm^3, generally increasing down to a depth of 240 cm, before decreasing slightly to the bottom of the core. The surface density of 14-6g is 1.32 g/cm^3. Density increase to 1.66 g/cm^3 at a depth of 60 cm, before decreasing to 1.37 at 68

cm, and remains relatively stable between 1.24 and 1.45 g/cm^3 down to the bottom at 220 cm. The surface density of 14-9g is 2.04 g/cm^3. Density oscillates irregularly between 1.87 and 2.23 g/cm^3 for the top 60 cm, before stabilizing between values of 1.95 and 2.06 g/cm^3 to the bottom at 244 cm. There is a localized minimum of 1.74 g/cm^3 at 235 cm.

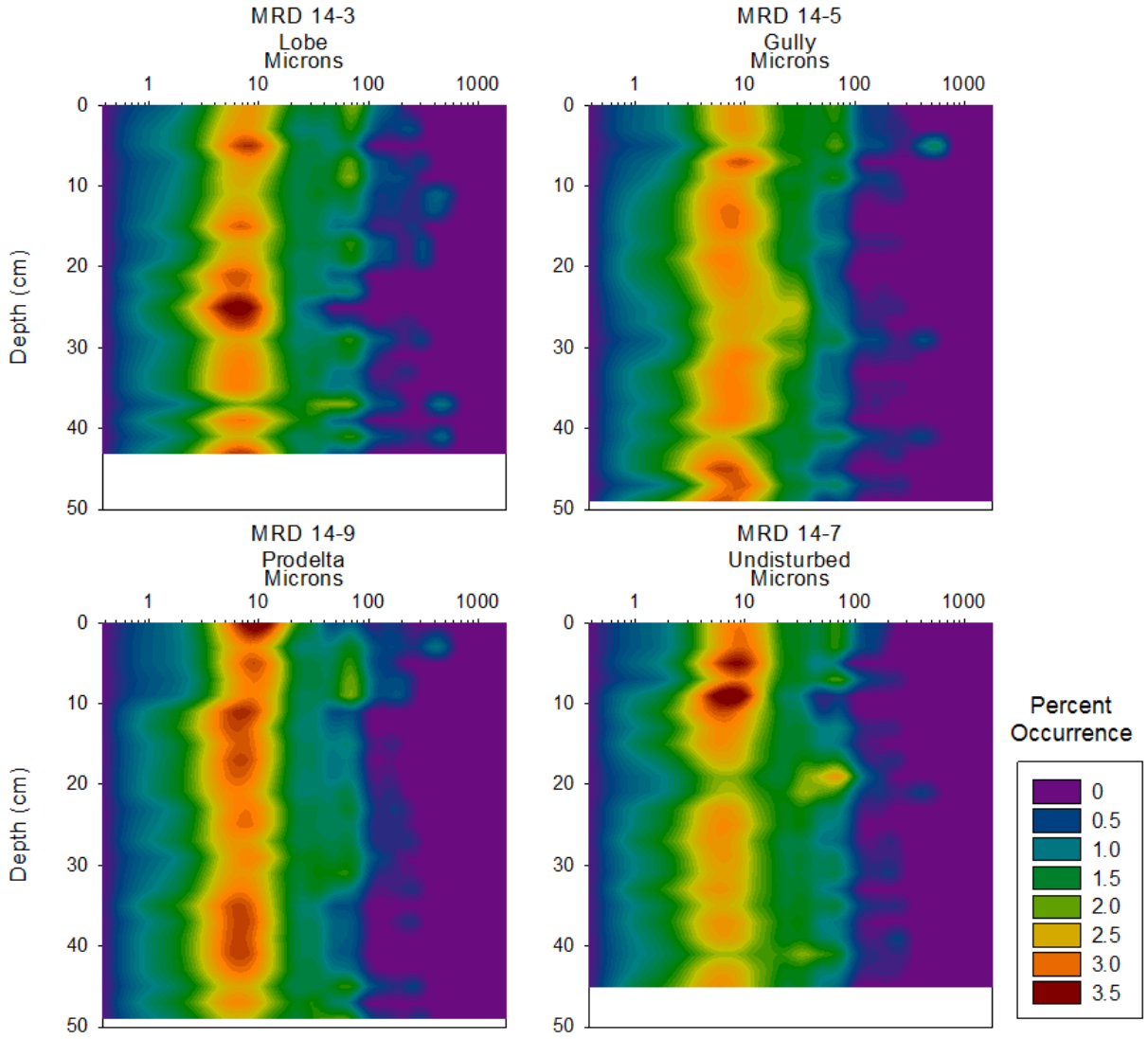

Figure 3: Selected grain size frequency plots. All four cores have a mode grain size in the very fine/fine silt range as displayed by warm colors, as well as a few layers slightly enriched in very fine/fine sand.

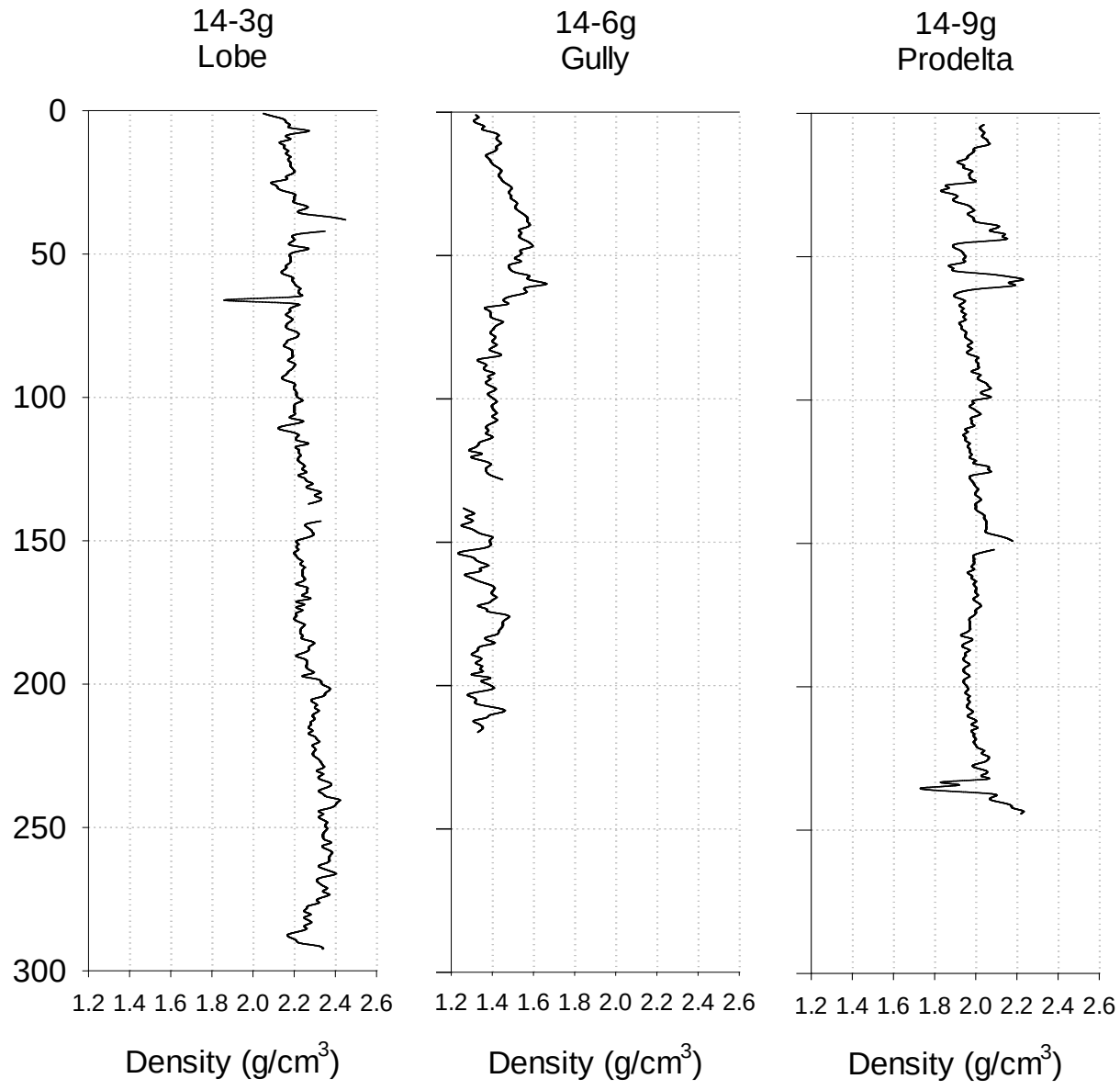

Figure 4: Downcore density profiles for the gravity cores. Core 14-6g has a low density layer beginning at 68 cm depth, corresponding with a layer of homogenized $^{210}Pb_{xs}$ activity. In all three cores, density variation decreases in the lower half of the cores.

4.3 Radionuclide Analysis

Results from ^{7}Be analysis are shown in Figure 5 (interpolated map of mass accumulation from ^{7}Be activity) and Figure 6 (activity profiles cores from proximal to distal locations, with

respect to SW Pass). Generally, both ^{7}Be inventories and penetration depths decrease away from the river mouth (Figures 5 and 6). Mass accumulation ranges from 1.2-8.7 g/cm^{2}.

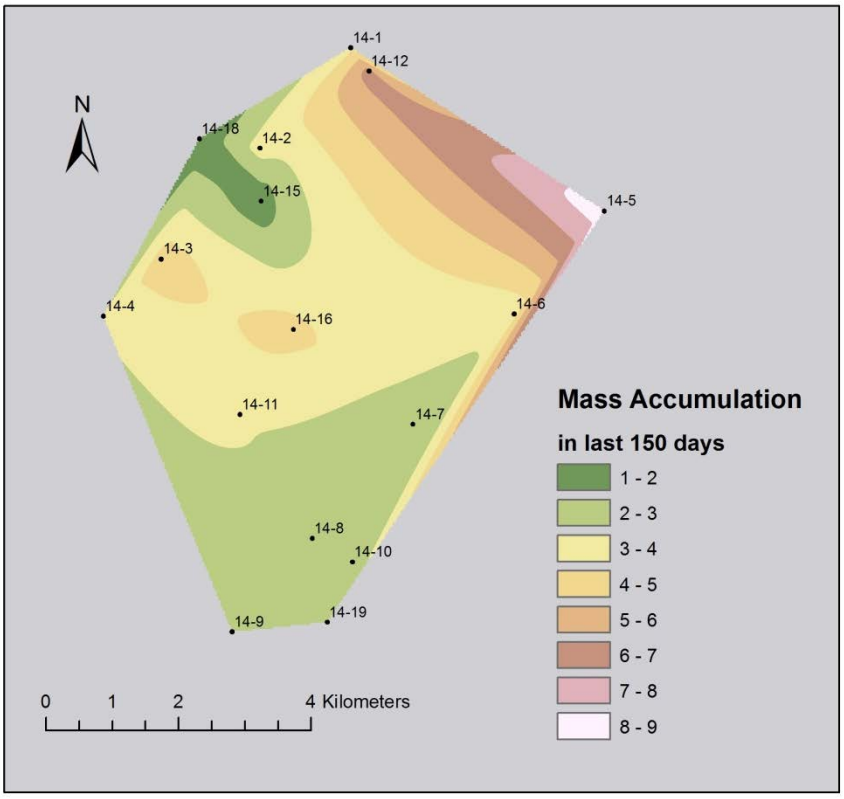

Figure 5: Mass accumulation of sediment via ^{7}Be activity. Results from each coring site were interpolated across the field area using Natural Neighbor Interpolation method. The highest values occur in the northeast side of the field area, closest to SW Pass.

Inventories range between 2.73 and 35.1 dpm/cm^{2}. Penetration depths range from 2 to 16 cm. Beryllium activity is coincident with a low bulk density drape. There is no apparent relation between mass accumulation, penetration depth or inventory with facies (undisturbed, gully, mudflow lobe, and prodelta). Proximity to SW Pass appears to be a primary control on ^{7}Be activity, penetration depth, and inventory (table 1).

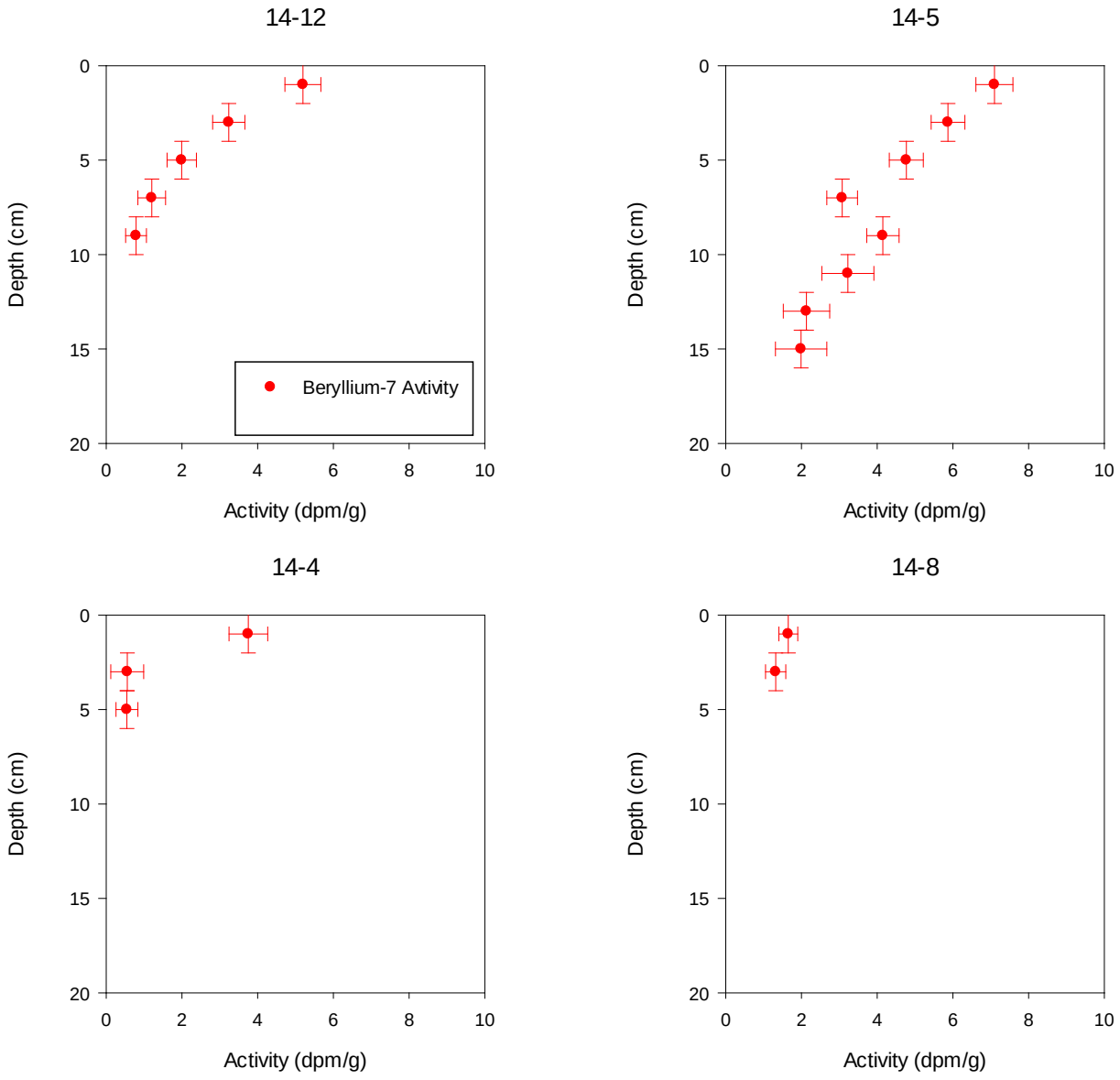

Figure 6: Selected ^{7}Be activity profiles. 14-5 and 14-12 were taken from the northeastern-most part of the field area and display the greatest depth of ^{7}Be penetration. Cores 14-4 and 14-8 were taken farther from SW Pass, and display less ^{7}Be penetration.

Table 1: Summary of radionuclide data of multicore samples

Station	Distance from SW (km)	Facies	^{7}Be Inventory (dpm/cm^{2})	^{7}Be Pentration Depth (cm;±1)	^{210}Pb SAR (cm/y)	R^2
14-1	6.9	und	13.24	6	2.1	0.79
14-2	8.6	gul	10.76	6	2.8	0.21
14-3	10.4	lob	11.77	8	2.3	0.59
14-4	11.6	pro	4.08	6	2.9	0.79
14-5	5.27	gul	34.06	16	40.7	0.01
14-6	7.26	gul	6.57	6	2.8	0.61
14-7	9.38	und	2.85	4	1.5	0.86
14-8	11.54	lob	2.73	4	1.7	0.58
14-9	13.32	pro	6.26	6	2.4	0.62
14-10	11.6	und	4.51	4	2.4	0.79
14-11	10.9	lob	5.96	6	2.7	0.32
14-12	6.7	gul	15.73	10	1.3	0.68
14-15	8.8	gul	2.30	2	1.6	0.61
14-16	9.4	gul/lob	5.47	8	3.7	0.32
14-18	9.2	gul	3.88	2	2.5	0.35
14-19	12.4	lob	3.45	4	5.3	0.06
Average			8.35	6.13	2.3	0.58

^{210}Pb SAR and R^2 averages were calculated without the values from cores 14-5 and 14-19 due to the poor fit to the data.

Excess Lead-210 ($^{210}Pb_{xs}$) declines gradually from highest activities at the sediment surface, with undulatory subsurface maxima and minima to the base of multicores, and in all gravity cores except for 14-6g. Surface activity (0-6 cm) generally ranges between 4 and 7 dpm/g with the lowest values occurring at sites closest to SW Pass in cores 14-1, 14-5, and 14-12 (Figures 1 and 7). Five cores have surface activity greater than 9 dpm/g, with the greatest activity, 12.2 dpm/g, occurring at a prodelta site (14-9) farthest from the river mouth (Figures 1 and 7). The majority of the low activity layers do not correspond with obvious variations in clay content (which scavenges the most ^{210}Pb; Cochran and Masqué, 2003). This trait is apparent in core 14-9, in the case of a low-activity layer at 22-32 cm depth for which there is no prominent

grain size difference compared with sediments above or below (Figures 3 and 7, lower left panel in each). One prominent exception to this observation is shown in Figure 8, where a low-activity zone in gravity core 14-3g coincides with the highest measured sand content in this study.

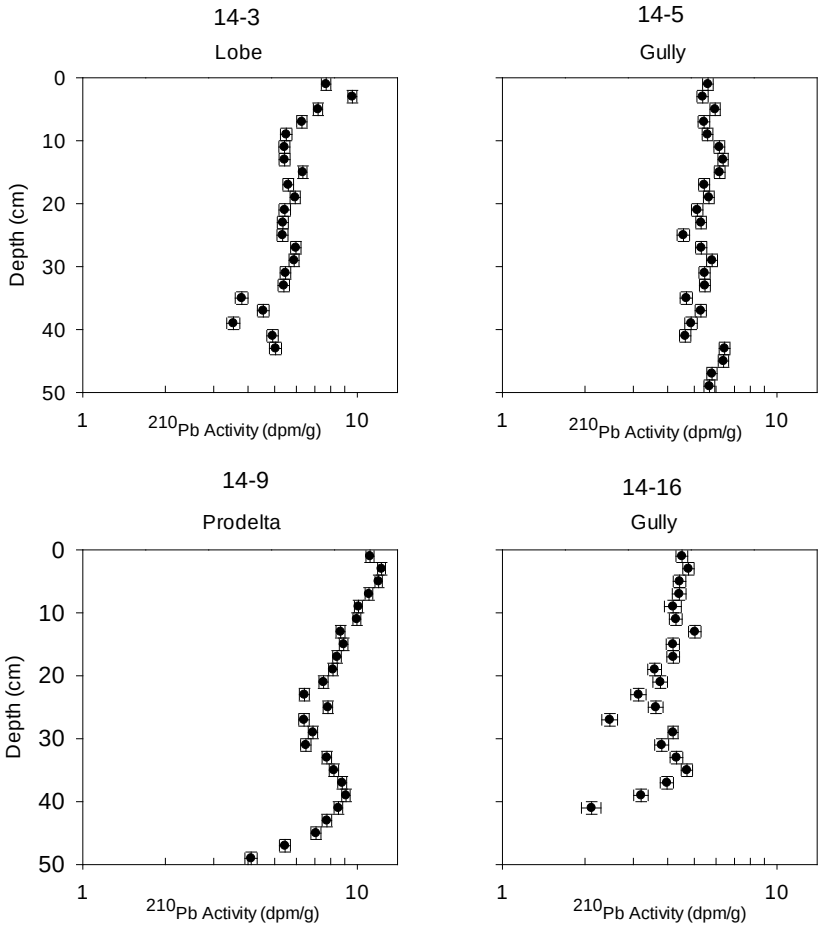

Figure 7: Selected ^{210}Pb activity profiles. These four examples display the varied nature of surface activity as well as the presence and absence of mid-core minima.

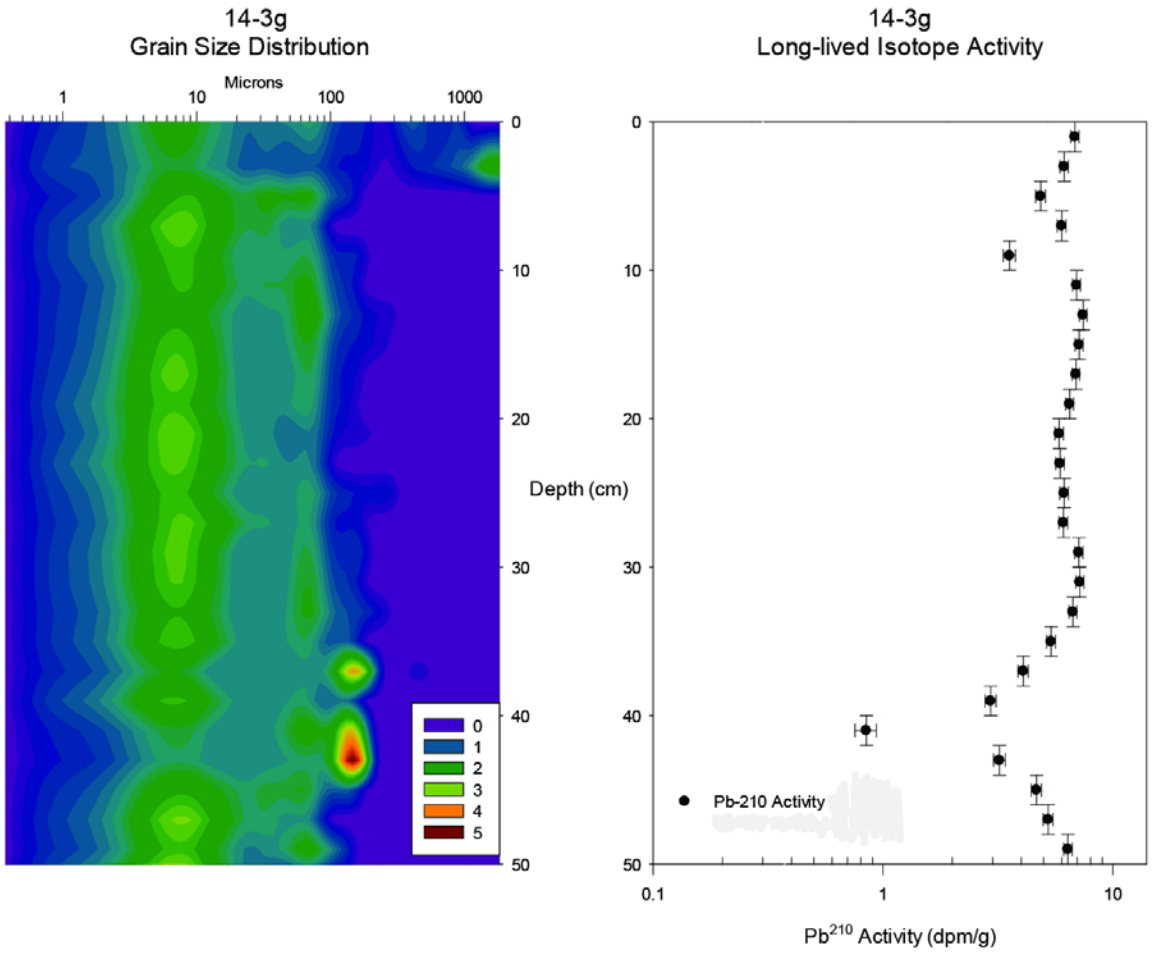

Figure 8: Summary of top 50 cm of 14-3g. Grain size is shown on the left and $^{210}Pb_{xs}$ activity on the right. There are two layers of decreased $^{210}Pb_{xs}$ activity, one between 8-10 cm, and between 36-44 cm. The 8-10 cm layer does not correlate with a change in grain size, however the lower horizon corresponds with the highest sand content measured in any sample from this study.

Sediment accumulation rates calculated from Equation 2 ranged from 1.5 to 3.7 cm/y measured using $^{210}Pb_{xs}$ activity in 14 multicores. Two values were disregarded due to an r^2 value of less than 0.1. On average, sediment accumulation rates calculated using $^{210}Pb_{xs}$ activity are 2.6 times lower than rates calculated using ^{7}Be (Table 1).

Sediment accumulation rates calculated with $^{210}Pb_{xs}$ activity from the gravity cores are noticeably greater than rates from the multicores (Table 2). Cores 14-3g, 14-6g, and 14-9g have rates of 6.0 (0-292 cm), 5.4 cm/y (0-90 cm) and 7.4 cm/y (0-246 cm) respectively. Activity

steadily decreases with depth for the entirety of core 14-3g, which is from a depositional lobe (Figure 9). There is a pattern of alternating higher and lower activity layers superimposed on this trend. There is also a steady decrease of activity across the top 70 cm of core 14-6g, which is from a mudflow gully. The alternating layers of high and low activity are less pronounced than in 14-3g. The sediment displays less heterogeneous activity below this depth to the bottom of the core (220 cm; Figure 9). Activity steadily decreases with depth in 14-9g, however, sampling sparse density does not allow for comment on the presence or absence of the undulatory behavior observed in other cores (Figure 9).

Table 2: Comparison between gravity core and multicore SAR

Core	Facies	^{210}Pb SAR (cm/y)	R^2
14-3	lob	2.3	0.59
14-3g	lob	6	0.56
14-6	gul	2.8	0.61
14-6g	gul	3.9	0.63
14-9	pro	2.4	0.62
14-9g	pro	7.4	0.75

Cesium-137 was detected in every sample from multicores and gravity cores that underwent radionuclide analysis, to the base of each core. No prominent subsurface maxima (used as a time marker for the 1963 ^{137}Cs maximum environmental release; Robbins and Edgington, 1975) were observed in any ^{137}Cs profiles. The presence of ^{137}Cs at the core-bottom depth of 292 cm in core 14-3g indicates a sediment accumulation rate of >4.87 cm/year since ca. 1954 (Robbins and Edgington, 1975), which is consistent with rates calculated using $^{210}Pb_{xs}$.

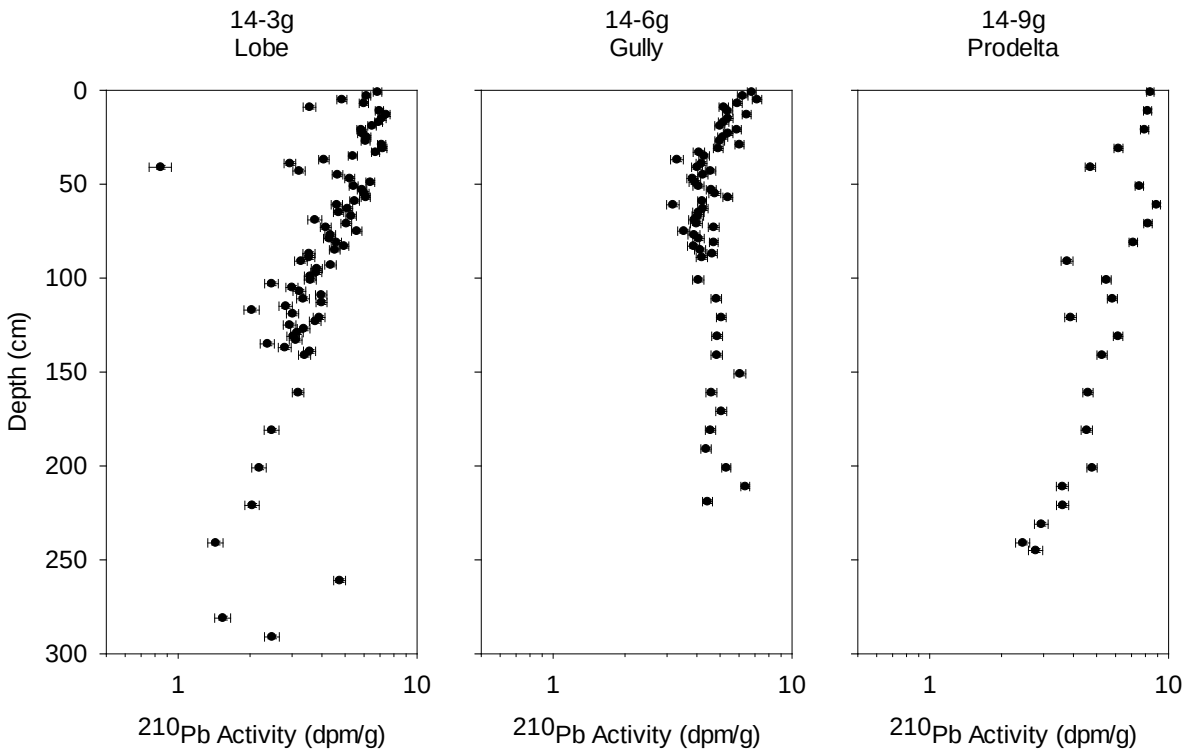

Figure 9: ^{210}Pb profiles for gravity cores. 14-3g (lobe), 14-6g (gully), 14-9g (prodelta). Activity steadily declines for the entirety of 14-3g and 14-9g. Activity decreases for the top 70 cm of 14-6g, before remaining constant for the remaining 150 cm of the core.

5 Discussion

The conveyance of sediment via river channels, dispersal in a receiving basin, and eventual deposition of sediment on the seafloor is driven primarily by turbulent jet diffusion, turbulent bed friction, and buoyant expansion, with waves and tides acting as secondary controls (Wright, 1977). Buoyant plumes form the primary method of sediment dispersal in river systems dominated by fine silts and clays in a microtidal regime with deep outlets (Wright, 1977)(Figure 10). The presence of a higher density salt wedge in the lower reaches of a river channel (observed in the lower MR; Wright and Coleman, 1974) enables the lower density river effluent to remain stratified and disperse sediment to the surrounding continental shelf. Initial sediment deposition may be followed by resuspension and transport before long-term accumulation (Wright and Nittrouer, 1995; Bentley, 2002). Continued transport after initial deposition can occur after resuspension into the water column, or by gravity driven flows near the sea-bed (Bentley, 2002). Wright and Nittrouer (1995) note that fairweather conditions on the MRDF do not retard the settling of sediment, and cannot resuspend it.

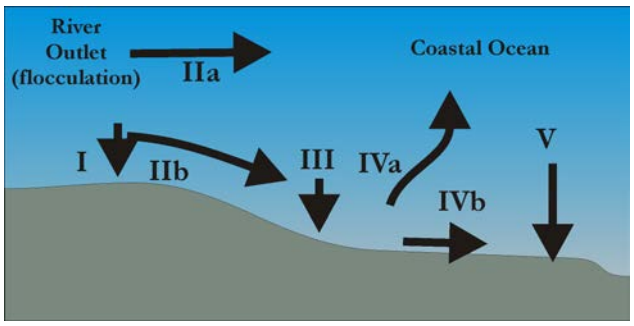

Figure 10: Patterns of fluvial sediment dispersal, deposition, and accumulation in the coastal ocean. After Wright and Nittrouer (1995) and Bentley (2002). Stage I: bedload deposition, bar formation; Stage IIa: seaward transport in buoyant plume; Stage IIb: seaward transport in hyperpycnal plume; Stage III: temporary deposition on shelf; Stage IVa: resuspension and transport in water column; Stage IVb: resuspension and transport in gravity-driven flow; Stage V: long-term accumulation.

Radiochemical indicators provide a useful tool to study both long and short term rates of sediment accumulation. ^{7}Be is a cosmogenic isotope that is brought to the surface by precipitation and concentrated in runoff from rivers. ^{7}Be has been used to assess recent (~6 months) flood deposits on continental shelves (Sommerfield et al., 1999; Young, 2014). ^{210}Pb is a product of the ^{238}U decay series and provides a longer record of sediment accumulation due to its 22.2 year half-life. Sommerfield and Nittrouer (1999) use ^{210}Pb to determine long term sediment accumulation rates on the California shelf near the Eel River. They also note that the clay rich layer deposited by the 1995 flood has lower overall activity, indicative of its fluvial source.

The rapid sedimentation recorded in the ^{7}Be of the multicore samples means that the relatively shallow multicores (< 60 cm) only record a few recent years of deposition. If the ^{7}Be sedimentation rates from 2014 are representative of previous years, the average age at the bottom of a multicore is 8.7 years. This finding helps to explain the lack of correlation between depositional environment and sedimentation rates. If there have not been mass failure events during the span captured in the multicores, there is no reason for depositional lobes to show consistently higher sedimentation than mudflow gullies, which are subject to removal of sediment or prodelta sites that do not receive input from mass failure events. Instead, plume dispersal processes (Figure 10) should dominate.

Trends in the surface $^{210}Pb_{xs}$ activity also indicate that deposition of sediment from plumes generated by the MR are the dominant driver of sedimentation over the recent period captured in the multicore samples. Sommerfield and Nittrouer (1999) demonstrate that rapidly deposited sediment on the continental shelf from the 1995 flood on the Eel River retained the

signal of a terrestrial source (low $^{210}Pb_{xs}$ activity) due to rapid deposition before substantial scavenging of ^{210}Pb could occur in the water column. Averaged $^{210}Pb_{xs}$ activity of the 2014 MR flood deposit (identified by ^{7}Be activity) increases with distance from SW pass, demonstrating the increased effect of scavenging of ^{210}Pb as the sediment plume disperses (Figure 11). The documented subsurface layers with decreased $^{210}Pb_{xs}$ activity with unchanging clay fraction may be further evidence of plume deposition. Years with particularly large river discharge such as 2011 may dilute seawater enough to lower scavenging rates over the field area, resulting in lower $^{210}Pb_{xs}$ activity without changes to grain size. These results indicate that the dominant mode of sedimentation is the annual input of sediment distributed across the field area with proximal sites receiving more than distal sites, regardless of the seafloor facies (which are controlled primarily by distribution of mass failures, not suspension settling from the plume).

The gravity cores provide a much longer record of activity, yielding long term sediment accumulation rates. Sediment accumulation rates calculated where a regression (Eq. 2) could be properly fitted to the data are generally in agreement with average sedimentation rates from ^{7}Be in the multicores. The convergence of long term $^{210}Pb_{xs}$ accumulation rates with short term ^{7}Be rates confirm that much of the deposited sediment is not removed without the presence of high stresses on the seafloor caused by hurricanes. Another line of evidence for the lack of mass failures captured is the presence of multiple packages of low activity layers stacked along a trend line that decreases with depth. $^{210}Pb_{xs}$ activity profiles indicate that sediment accumulation rates do not vary greatly with facies over longer scales than were captured in the multicores with one exception, detailed below.

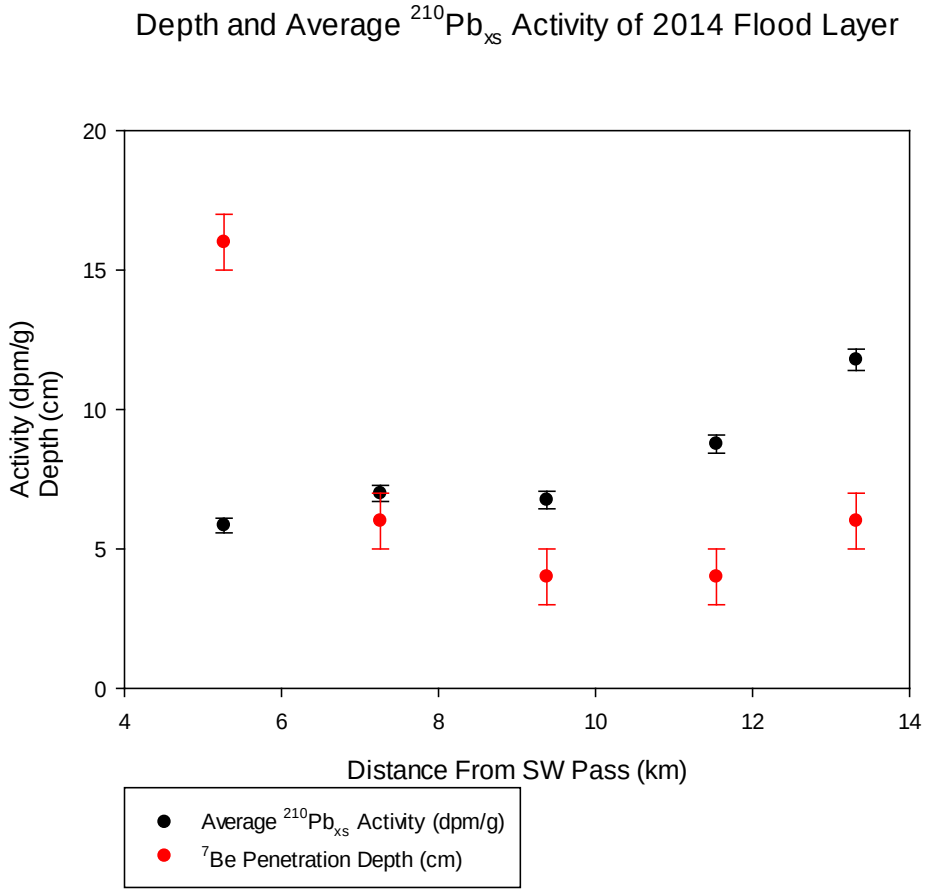

Figure 11: Averaged ^{210}Pbxs activity associated with 2014 flood layer. Red circles indicate depth of ^{7}Be penetration, which decreases in cores father from SW pass. Black circles indicate the average $^{210}Pb_{xs}$ activity of the samples for which ^{7}Be was present. Average activity increases with distance from SW Pass, indicating the increased signal of lead scavenging from seawater.

Coleman et al.(1980) describe rapid and episodic advancement of mudflow lobes when the corresponding gully system is active followed a lack of progradation coupled with a thin cap settling out of river plumes. The data collection methods of Coleman et al. (1980) involved repeated seafloor surveys using sidescan and sub-bottom sonar. A sediment accumulation rate of 6.0 cm/y was calculated using samples from 0-292 cm from core 14-3g, which is in agreement with average sediment accumulation rates across the area using ^{7}Be, indicating no sediment was received from mass failures in the last ~49 years (encompassing hurricanes Betsy [1965], Camille [1969], Ivan [2004], and Katrina [2005]). While this core did not penetrate deep

enough to capture a layer of homogenized mud deposited by mass failure, the sediment record from the top of the mudflow lobe supports Coleman et al.'s (1980) model of punctuated, rapid movement followed by periods of relative stability.

In core 14-6g, the sediment accumulation from $^{210}Pb_{xs}$ activity with the best fit is over the interval 0-70 cm (3.9 cm/year), which is in agreement with average river plume sediment accumulation rates. Scavenging effects do appear in this upper section of the core, consistent with other cores in the area. From this depth to the bottom of the core at 246 cm, the sedimentation equation does not yield a good fit to the data, and the calculated sediment accumulation rate rises to 19.13 cm/yr. Regressions using Eq. 2 for ^{210}Pb become less reliable at such high accumulation rates, owing to the sensitivity of the equation to slight gradient changes in ^{210}Pb activity versus depth (Hirschberg and Schubel, 1979). Although this rate is unlikely to represent actual sediment accumulation rates, the poor fit of the line indicates that the observed $^{210}Pb_{xs}$ activity is not explained by steady-state deposition of sediment over long periods of time. Although sample density in this core section is lower than for upper sections, ^{210}Pb activity in the lower layer of the core appears more homogenous, which is likely indicative of rapid/instantaneous deposition or physical reworking (Nittrouer et al., 1984). These sediments likely represent a mudflow that deposited at least 176 cm of sediment.

Core 14-9g was collected from beyond the extent of the mudflow gullies and depositional lobes; the sediment accumulation rate (7.4 cm/year) calculated using this whole core is in agreement with ^{7}Be rates (Figure 9). The resolution of the gravity core data at this site does not allow for the confirmation of scavenging effects, however fluctuations in $^{210}Pb_{xs}$ activity present in the multicore samples from this station are not as pronounced as in cores

closer to the mouth of SW Pass. It is likely that given the distance from SW Pass, there is less annual variability in the strength of river plume signal (low $^{210}Pb_{xs}$ activity) as it reaches this station, leading to less variability in $^{210}Pb_{xs}$ activity.

The best evidence of a mass flow is captured in 14-6g. The homogenization of $^{210}Pb_{xs}$ activity begins at a depth of 70 cm, which is coincident with a drop in density captured by the whole core logger. Coleman et al. (1980) describe the movement of blocks with intact stratigraphy as well as remolded sediments which are acoustically transparent in sonar images. The data from this core suggest that it was collected from a region of the seafloor that was remolded. Using ^{7}Be and ^{210}Pb sediment accumulation rates for upper and lower bounds, the flow occurred between 9 and 18 years ago, a period during which 7 tropical cyclones passed within 100 km of the field area, including Katrina in 2005. Strong sea-floor shear stresses associated with hurricanes are likely needed to drive mass failures on the upper delta front. However, bottleneck slides and mudflow gullies were observed by Denommee and Bentley (in press) in much shallower waters (<10 m) triggered by strong cold front passages on the Atchafalaya shelf, underscoring the importance of mass wasting events in sediment redistribution along muddy continental shelves.

6 Conclusions

This study provides insight on the geochronology of the upper delta front of the Mississippi river, in particular the signals of recent deposition and mass failure. Analysis of sediment cores from four depositional environments provided a multi-faceted approach to the study of mass wasting events and accumulation patterns. The significant findings can be summarized as follows:

1) ^{7}Be activity shows that 2-16 cm of sediment was delivered to the study area by the MR during the spring flood of 2014 prior to core collection. Sedimentation rates are highest near the SW Pass distributary, and do not correlate to depositional environments.
2) $^{210}Pb_{xs}$ activities associated with the 2014 flood layer are variable and increase with distance from SW Pass. There are several layers preserved in multicores and gravity cores of decreased $^{210}Pb_{xs}$ activity that do not correlate with changes in clay fraction. These data suggest that the amount of lead scavenging varies annually and spatially in the field area.
3) $^{210}Pb_{xs}$ sediment accumulation rates calculated in the multicores (2.33 cm/y) were on average 2.6 times lower than ^{7}Be sedimentation rates (6.13 cm/y) from the same core. $^{210}Pb_{xs}$ sediment accumulation rates from the longer gravity cores (avg. 5.65 cm/y) are higher and more similar to ^{7}Be rates, indicating the effects of the variable activity of the annual flood layer due to scavenging are averaged out over time.
4) Mass failures can be detected by their physical properties preserved in sediment cores. No evidence was recorded in the short multicores, however a layer of

homogenized $^{210}Pb_{xs}$ activity corresponding with a layer of low densities from a core recovered from a mudflow gully. There was no such layer recorded in the gravity core from a mudflow lobe, however other studies (Coleman et al., 1980) note that older flows were covered by river plume deposits with internal stratigraphy. This finding confirms that episodic mass wasting events can affect just one gully/lobe system, and not the entire sea floor.

5) Future studies may benefit by targeting areas on the delta front with lower sedimentation rates. SW Pass discharges more sediment than South Pass and Pass a Loutre combined, which may bury mudflows under a thick package of river plume deposits. Additionally, collecting a high resolution core transect across one gully and lobe system may provide insight to the evolution of a mudflow downslope.

7 References

Allison, M. A., Demas, C. R., Ebersole, B. A., Kleiss, B. A., Little, C. D., Meselhe, E. A., Powell, N. J., Pratt, T. C., and Vosburg, B. M., 2012, A water and sediment budget for the lower Mississippi–Atchafalaya River in flood years 2008–2010: Implications for sediment discharge to the oceans and coastal restoration in Louisiana: Journal of Hydrology, v. 432-433, p. 84-97.

Allison, M. A., Sheremet, A., Goni, M. A., and Stone, G. W., 2005, Storm layer deposition on the Mississippi-Atchafalaya subaqueous delta generated by Hurricane Lili in 2002: Continental Shelf Research, v. 25, no. 18, p. 2213-2232.

Bentley Sr, S. J., 2002, Dispersal of fine sediments from river to shelf: process and product.

Bentley Sr, S. J., Blum, M. D., Maloney, J., Pond, L. G., and Paulsell, R. L., 2015, The Mississippi River Source to Sink System: Perspectives on Tectonic, Climatic, and Anthropogenic Influences, Miocene to Anthropocene: Invited review in revision, Earth Science Reviews.

Blum, M. D., and Roberts, H. H., 2009, Drowning of the Mississippi Delta due to insufficient sediment supply and global sea-level rise: Nature Geosci, v. 2, no. 7, p. 488-491.

Blum, M. D., and Roberts, H. H., 2012, The Mississippi Delta Region: Past, Present, and Future: Annual Review of Earth and Planetary Sciences, v. 40, p. 655-683.

Cochran, J. K., and Masqué, P., 2003, Short-lived U/Th Series Radionuclides in the Ocean: Tracers for Scavenging Rates, Export Fluxes and Particle Dynamics: Reviews in Mineralogy and Geochemistry, v. 52, no. 1, p. 461-492.

Coleman, J. M., Prior, D. B., and Garrison, L. E., 1978, Submarine Landslides In The Mississippi River Delta: Proceedings of the Offshore Technology Conference, v. 10, no. 3170.

Coleman, J. M., Prior, D. B., and Garrison, L. E., 1980, Subaqueous sediment instabilities in the offshore Mississippi River delta: U.S. Department of the Interior, Bureau of Land Management.

Coleman, J. M., Roberts, H. H., and Stone, G. W., 1998, Mississippi River Delta: An Overview: Journal of Coastal Research, v. 14, no. 3, p. 698-716.

Corbett, D. R., McKee, B., and Allison, M. A., 2006, Nature of decadal-scale sediment accumulation on the western shelf of the Mississippi River delta: Continental Shelf Research, v. 26, no. 17-18, p. 2125-2140.

Corbett, D. R., McKee, B., and Duncan, D., 2004, An evaluation of mobile mud dynamics in the Mississippi River deltaic region: Marine Geology, v. 209, no. 1-4, p. 91-112.

Galloway, W. E., 1975, Process framework for describing the morphologic and stratigraphic evolution of deltaic depositional systems.

Guidroz, W. S., 2009, Subaqueous, hurricane-initiated shelf failure morphodynamics along the Mississippi River Delta Front, North-Central Gulf of Mexico [Doctor of Philosophy: Louisiana State University.

Hirschberg, D. J., and Schubel, J. R., 1979, Recent geochemical history of flood deposits in the northern Chesapeake Bay: Estuarine and Coastal Marine Science, v. 9, no. 6, p. 771-IN777.

Hooper, J. R., and Suhayda, J. N., 2005, Hurricane Ivan as a Geologic Force: Mississippi Delta Front Seafloor Failures: Proceedings of the Offshore Technology Conference, no. 17737.

Hülse, P., and Bentley Sr, S. J., 2012, A 210Pb sediment budget and granulometric record of sediment fluxes in a subarctic deltaic system: The Great Whale River, Canada: Estuarine, Coastal and Shelf Science, v. 109, p. 41-52.

Kaiser, M. J., Yu, Y., and Jablonowski, C. J., 2009, Modeling lost production from destroyed platforms in the 2004–2005 Gulf of Mexico hurricane seasons: Energy, v. 34, no. 9, p. 1156-1171.

Kemp, G. P., Willson, C. S., Rogers, J. D., Westphal, K. A., and Binselam, S. A., 2014, Adapting to change in the lowermost Mississippi River: Implications for navigation, flood control and restoration of the delta ecosystem, Perspectives on the Restoration of the Mississippi Delta, Springer, p. 51-84.

Lee, H. J., Greene, H. G., Edwards, B. D., Fisher, M. A., and Normark, W. R., 2009, Submarine landslides of the Southern California Borderland: Special Paper - Geological Society of America, v. 454, p. 251-269.

Maloney, J., Bentley Sr, S. J., Obelcz, J., Miner, M. D., Georgiou, I. Y., Hanegan, K., and Keller, G., 2014, Assessing Subaqueous Mudflow Hazard on the Mississippi River Delta Front, Part 1: A Historical Perspective on Mississippi River Delta Front Sedimentation: AGU Fall Meeting, p. Poster.

Meade, R. H., 1996, River-sediment inputs to major deltas, Coastal Systems and Continental Margins Volume 2: Sea-Level Rise and Coastal Subsidence: Netherlands, Kluwer Academic Publishers : Dordrecht - Boston - London, Netherlands, p. 63-85.

Muhammad, Z., Bentley, S. J., Febo, L. A., Droxler, A. W., Dickens, G. R., Peterson, L. C., and Opdyke, B. N., 2008, Excess 210Pb inventories and fluxes along the continental slope

and basins of the Gulf of Papua: Journal of Geophysical Research: Earth Surface (2003–2012), v. 113, no. F1.

Nittrouer, C. A., DeMaster, D. J., McKee, B. A., Cutshall, N. H., and Larsen, I. L., 1984, The effect of sediment mixing on Pb-210 accumulation rates for the Washington continental shelf: Marine Geology, v. 54, no. 3–4, p. 201-221.

Obelcz, J., Xu, K., Bentley Sr, S. J., Georgiou, I. Y., Maloney, J., Miner, M. D., Hanegan, K., and Keller, G., 2014, Assessing subaqueous mudslide hazard on the Mississippi River Delta Front, Part 2: Insights revealed by new high-resolution geophysical surveying: AGU Fall Meeting.

Prior, D. B., and Suhayda, J. N., 1979, Submarine Mudslide Morphology And Development Mechanisms, Mississippi Delta: Proceedings of the Offshore Technology Conference, no. 3482.

Robbins, J. A., and Edgington, D. N., 1975, Determination of recent sedimentation rates in Lake Michigan using Pb-210 and Cs-137: Geochimica et Cosmochimica Acta, v. 39, no. 3, p. 285-304.

Slingerland, R., Driscoll, N. W., Milliman, J. D., Miller, S. R., and Johnstone, E. A., 2008, Anatomy and growth of a Holocene clinothem in the Gulf of Papua: Journal of Geophysical Research: Earth Surface (2003–2012), v. 113, no. F1.

Sommerfield, C. K., and Nittrouer, C. A., 1999, Modern accumulation rates and a sediment budget for the Eel shelf: a flood-dominated depositional environment: Marine Geology, v. 154, no. 1, p. 227-241.

Sommerfield, C. K., Nittrouer, C. A., and Alexander, C. R., 1999, 7Be as a tracer of flood sedimentation on the northern California continental margin: Continental Shelf Research, v. 19, no. 3, p. 335-361.

Sterling, G. H., and Strohbeck, E. E., 1973, The Failure of the South Pass 70 "B" Platform Hurricane Camille: Proceedings of the Offshore Technology Conference, no. 1898.

Walsh, J. P., Corbett, D. R., Mallinson, D., Goni, M., Dail, M., Lowey, K., Marcinak, K., Ryan, K., Smith, C., Stevens, A., Sumners, B., and Tesh, T., 2006, Mississippi Delta Mudflow Activity and 2005 Gulf Hurricanes: Eos, Transactions, American Geophysical Union, v. 87, no. 44, p. 477-478.

Walsh, J. P., and Nittrouer, C. A., 2009, Understanding fine-grained river-sediment dispersal on continental margins: Marine Geology, v. 263, no. 1-4, p. 34-45.

Wang, D. W., Mitchell, D. A., Teague, W. J., Jarosz, E., and Hulbert, M. S., 2005, Extreme waves under Hurricane Ivan: Science, v. 309, no. 5736, p. 896-896.

WRIGHT, L. D., 1977, Sediment transport and deposition at river mouths: A synthesis: Geological Society of America Bulletin, v. 88, no. 6, p. 857-868.

Wright, L. D., and Coleman, J. M., 1974, Mississippi River Mouth Processes - Effluent Dynamics and Morphologic Development: Journal of Geology, v. 82, no. 6, p. 751-778.

Wright, L. D., and Nittrouer, C. A., 1995, Dispersal of River Sediments in Coastal Seas - 6 Contrasting Cases: Estuaries, v. 18, no. 3, p. 494-508.

Xu, K., Harris, C. K., Hetland, R. D., and Kaihatu, J. M., 2011, Dispersal of Mississippi and Atchafalaya sediment on the Texas-Louisiana shelf: Model estimates for the year 1993: Continental Shelf Research, v. 31, p. 1558-1575.

Young, D. R., 2014, Examination of the 2011 Mississippi River Flood Deposit on the Louisiana Continental ShelfMaster's Thesis]: East Carolina University.

Appendix I Additional Multicore Data

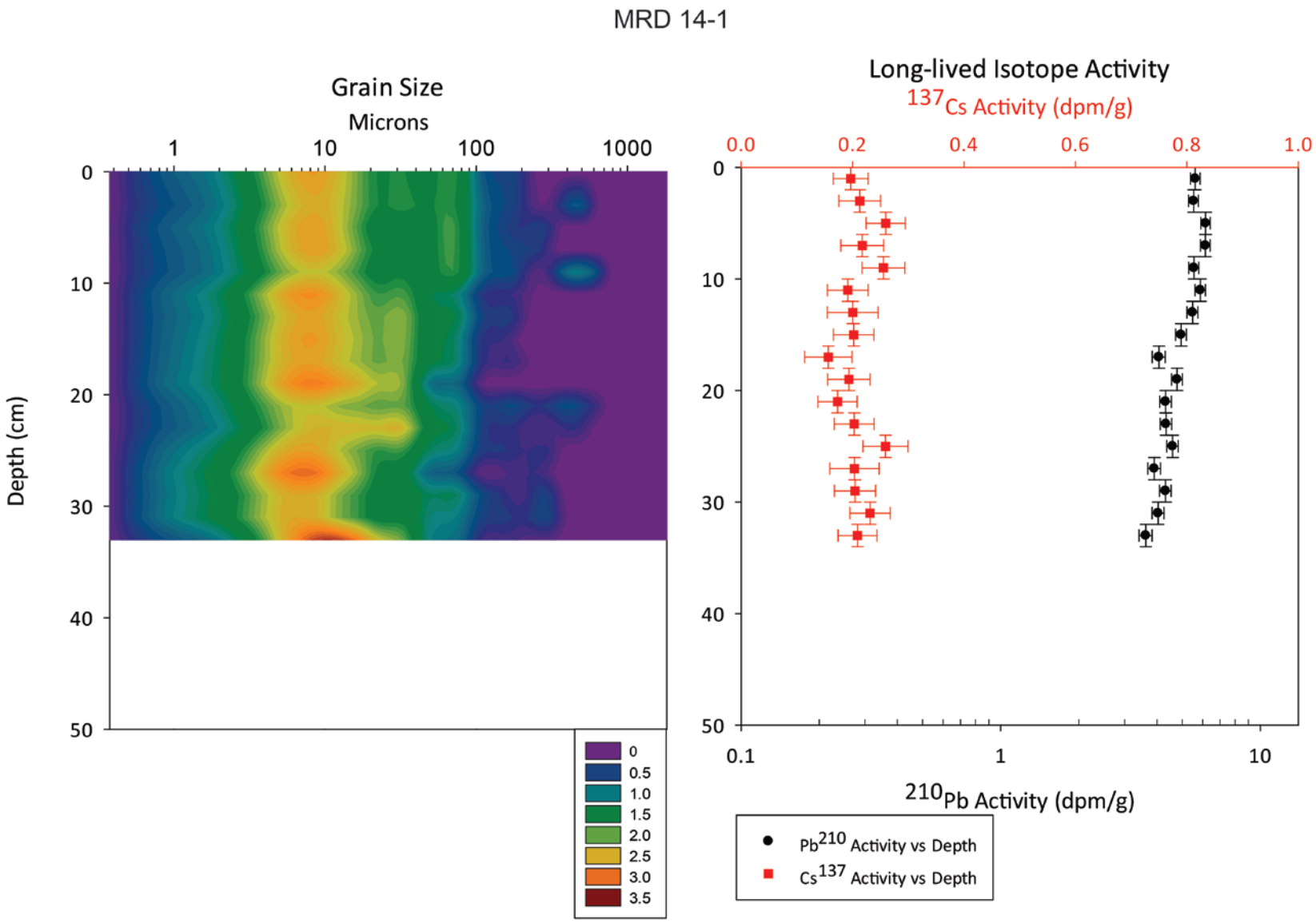

(Appendix I continued)

MRD 14-2

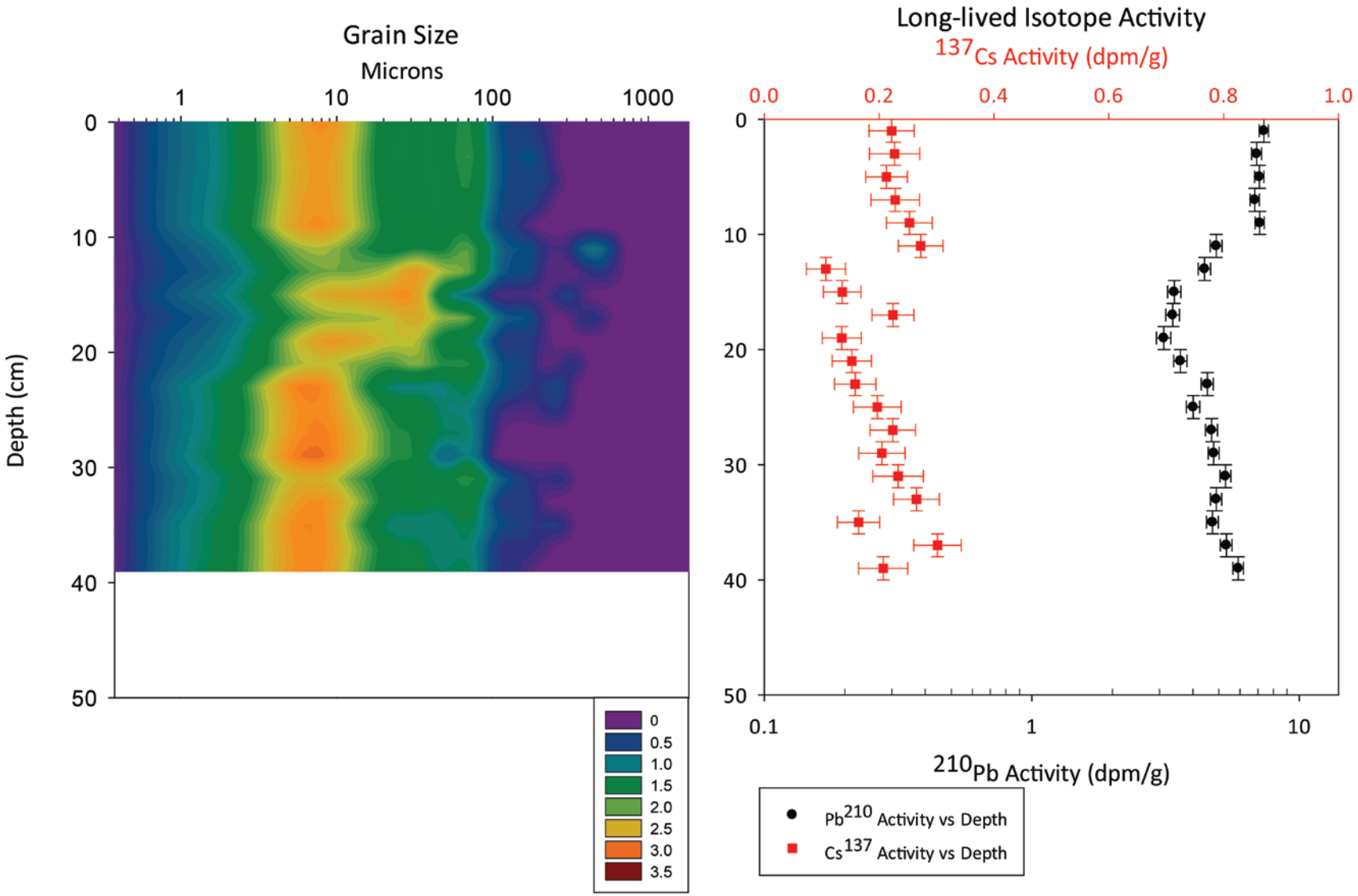

(Appendix I continued)

MRD 14-3

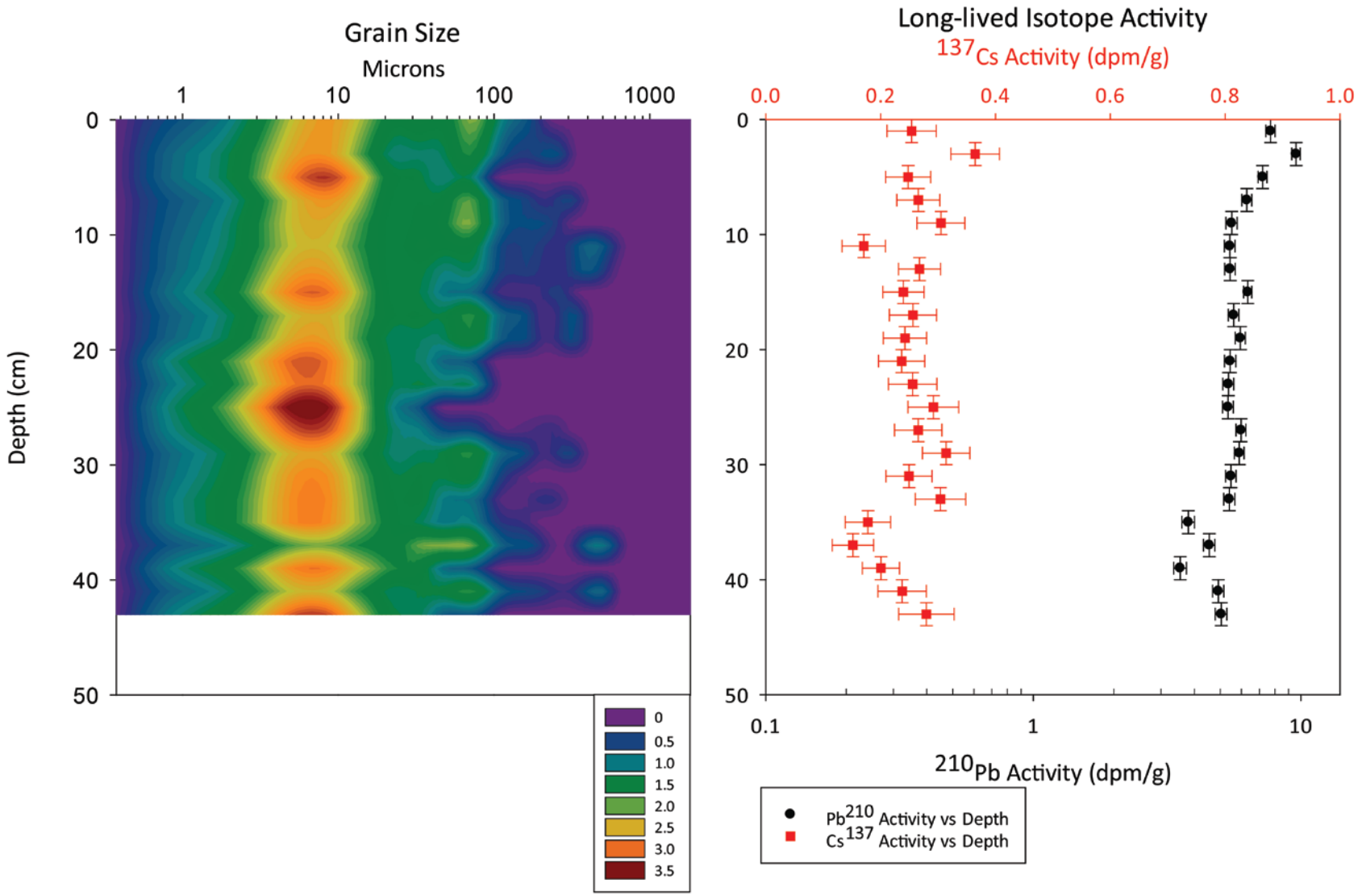

(Appendix I continued)

MRD 14-4

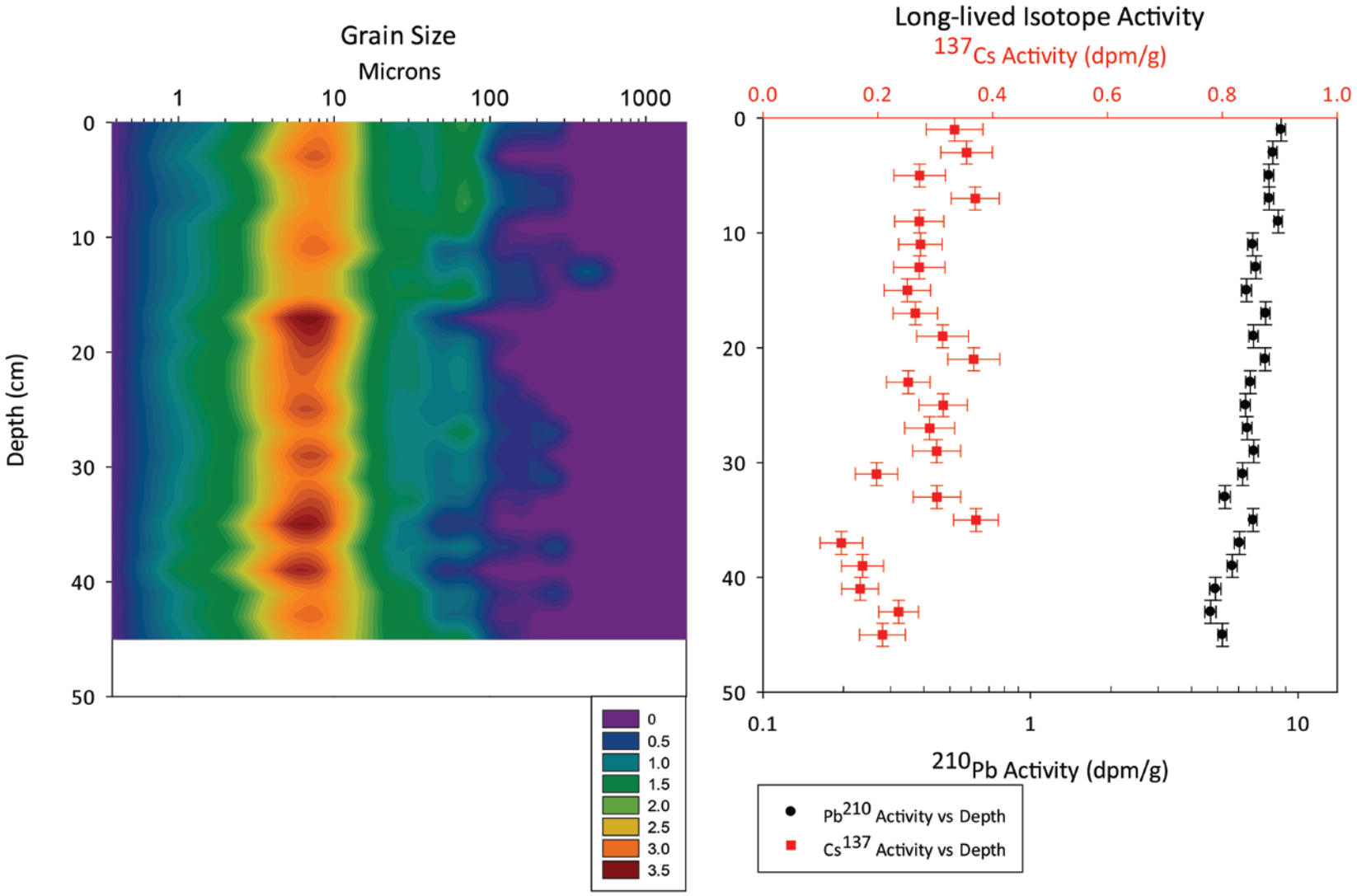

(Appendix I continued)

MRD 14-5

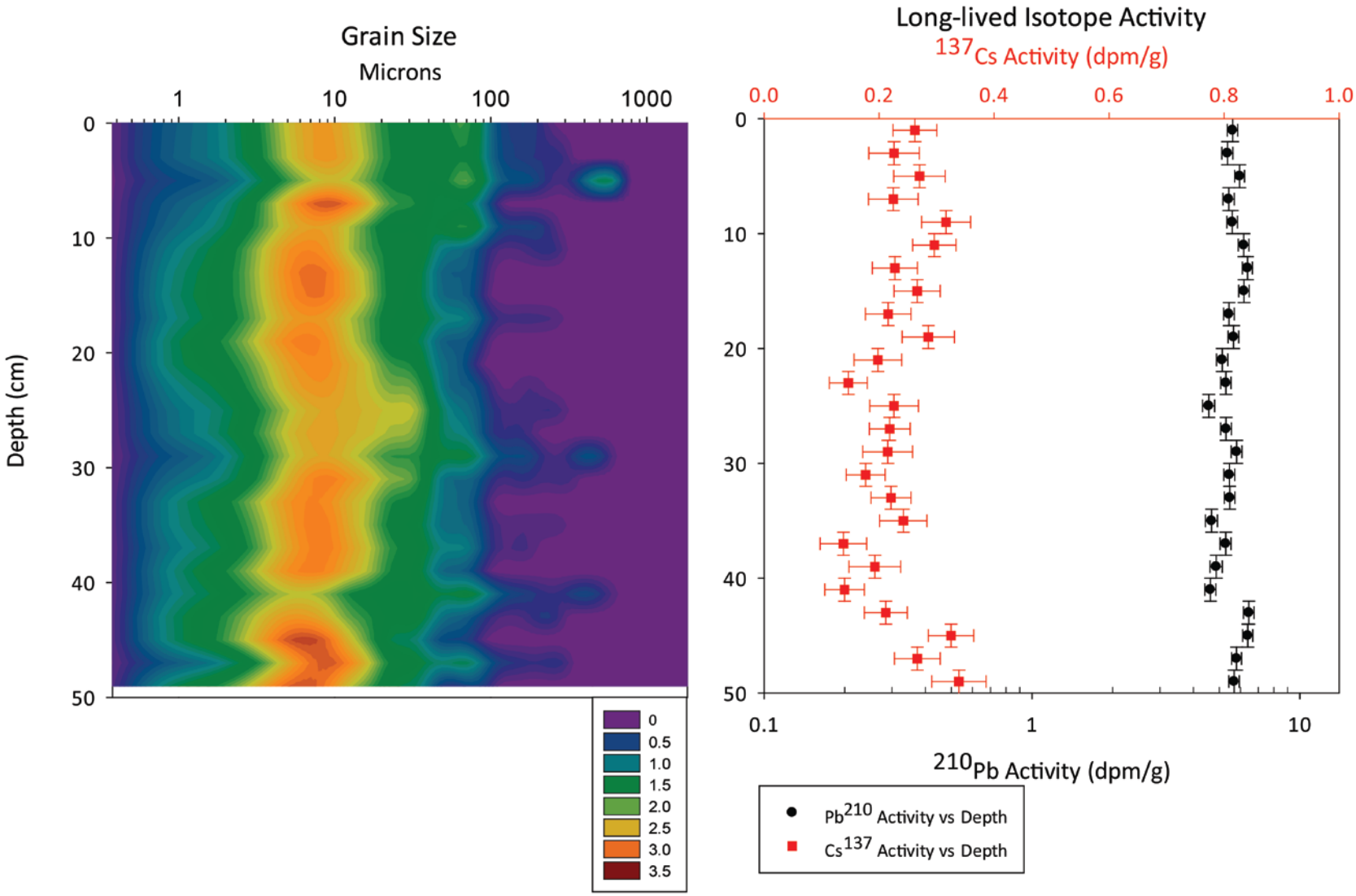

(Appendix I continued)

MRD 14-6

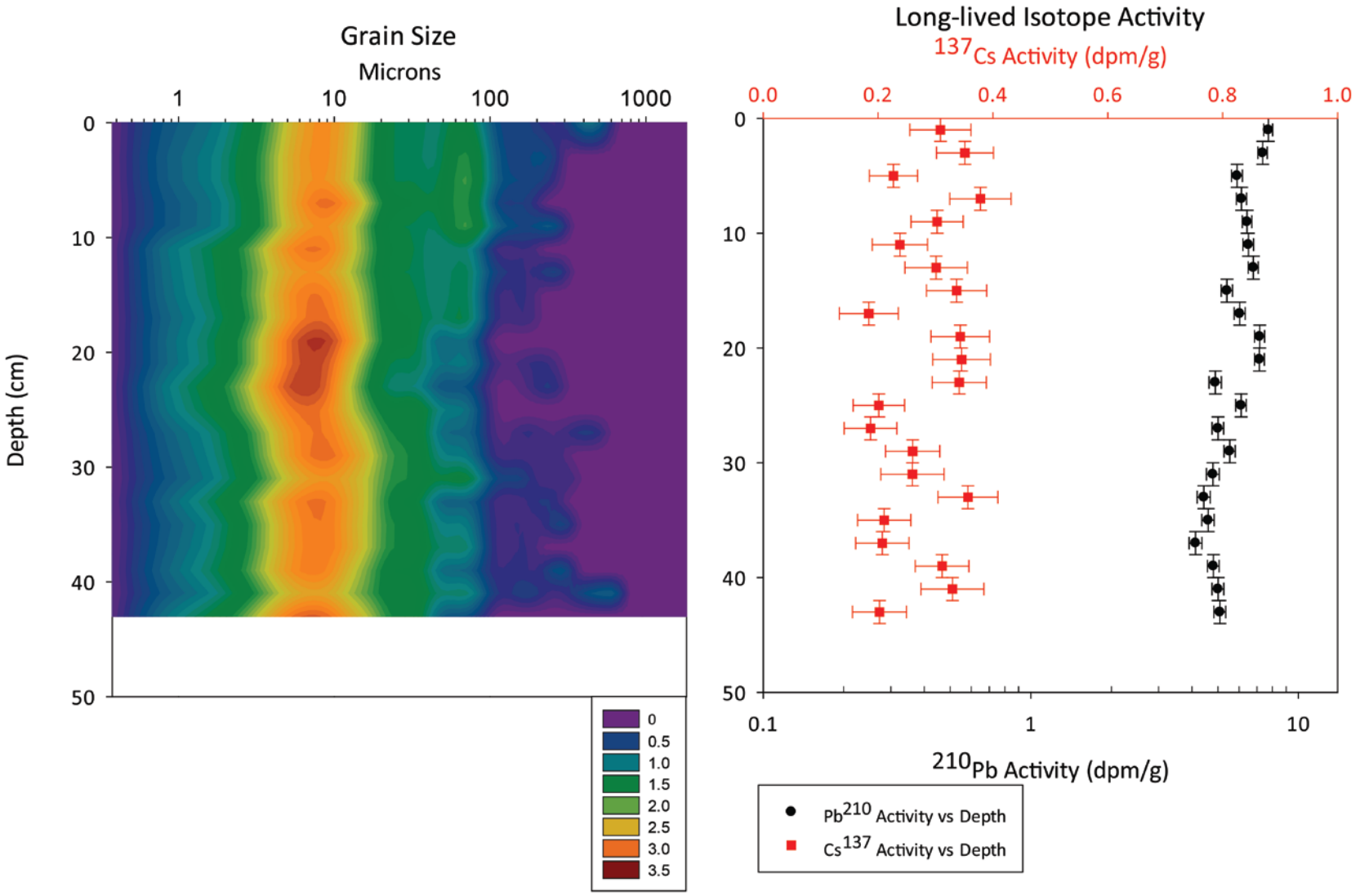

(Appendix I continued)

MRD 14-7

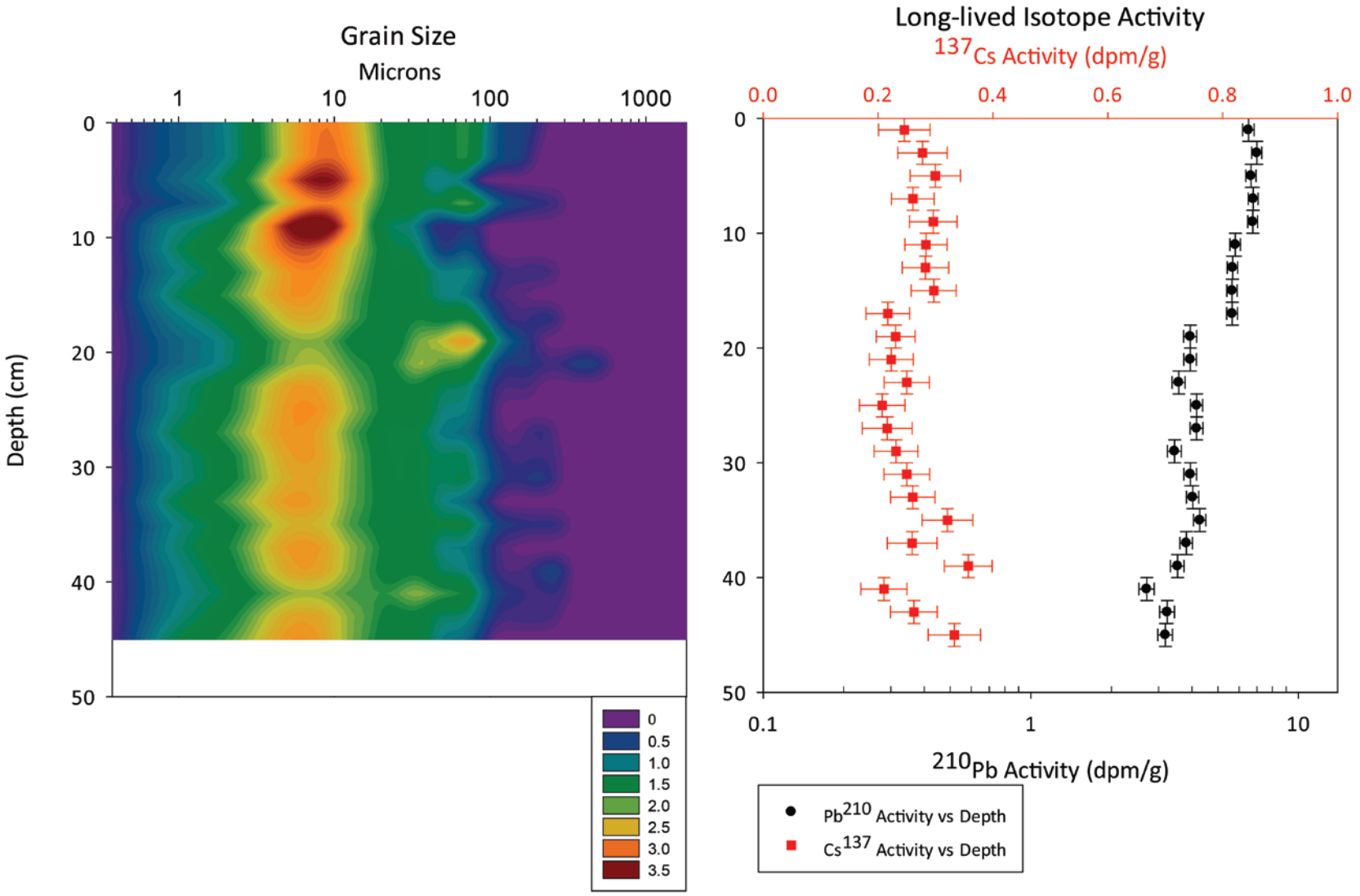

(Appendix I continued)

MRD 14-8

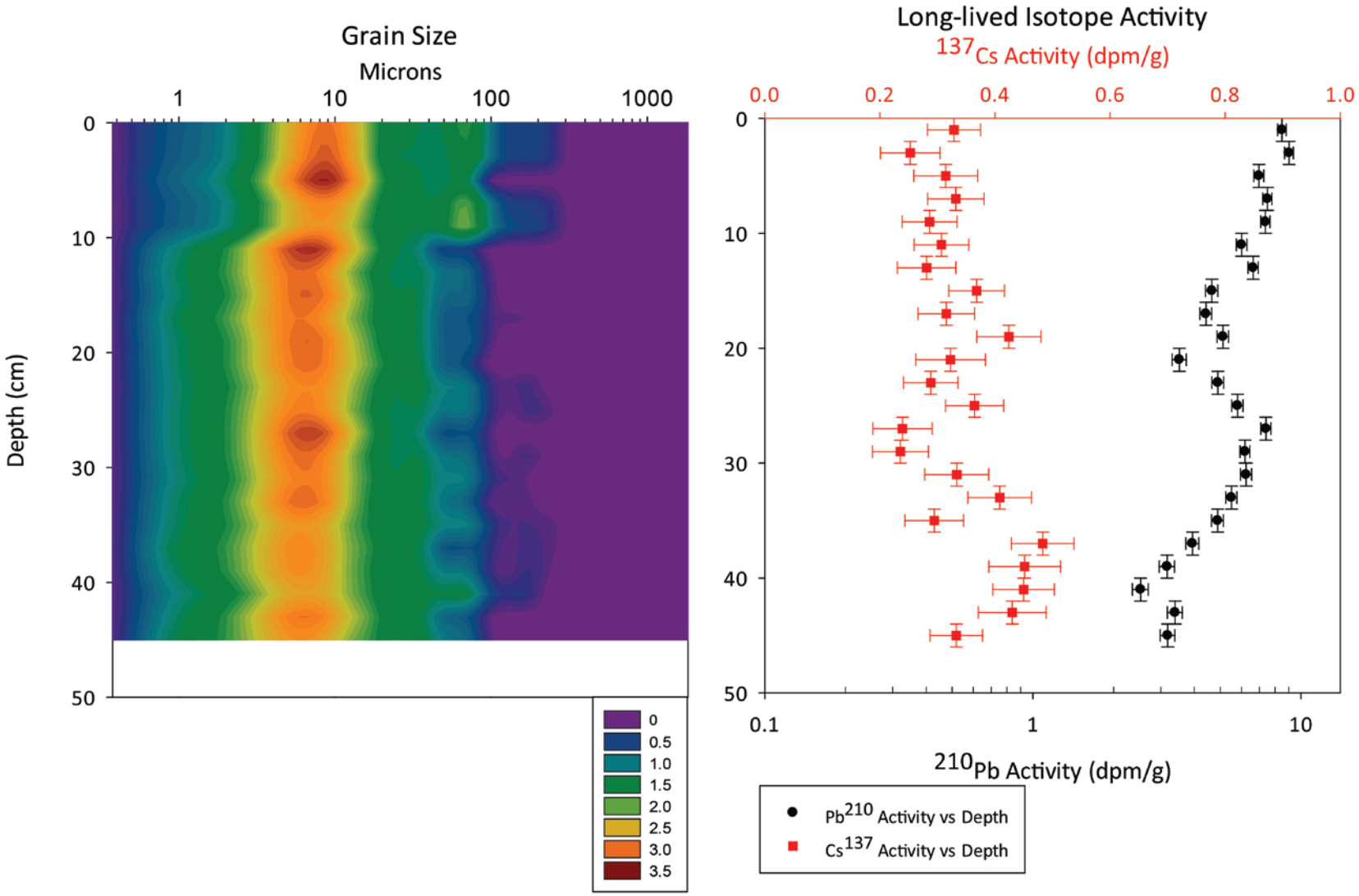

(Appendix I continued)

MRD 14-9

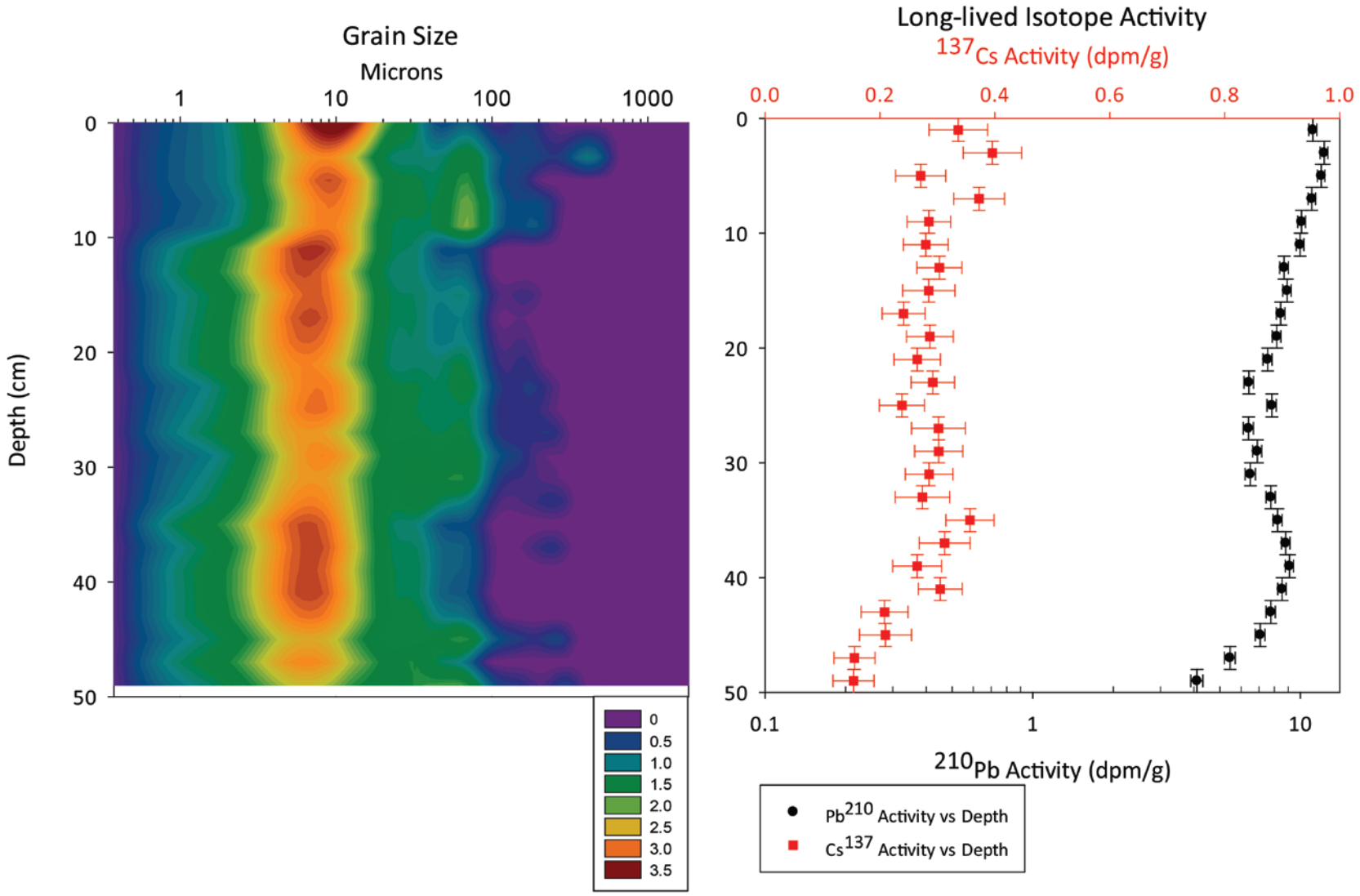

(Appendix I continued)

MRD 14-10

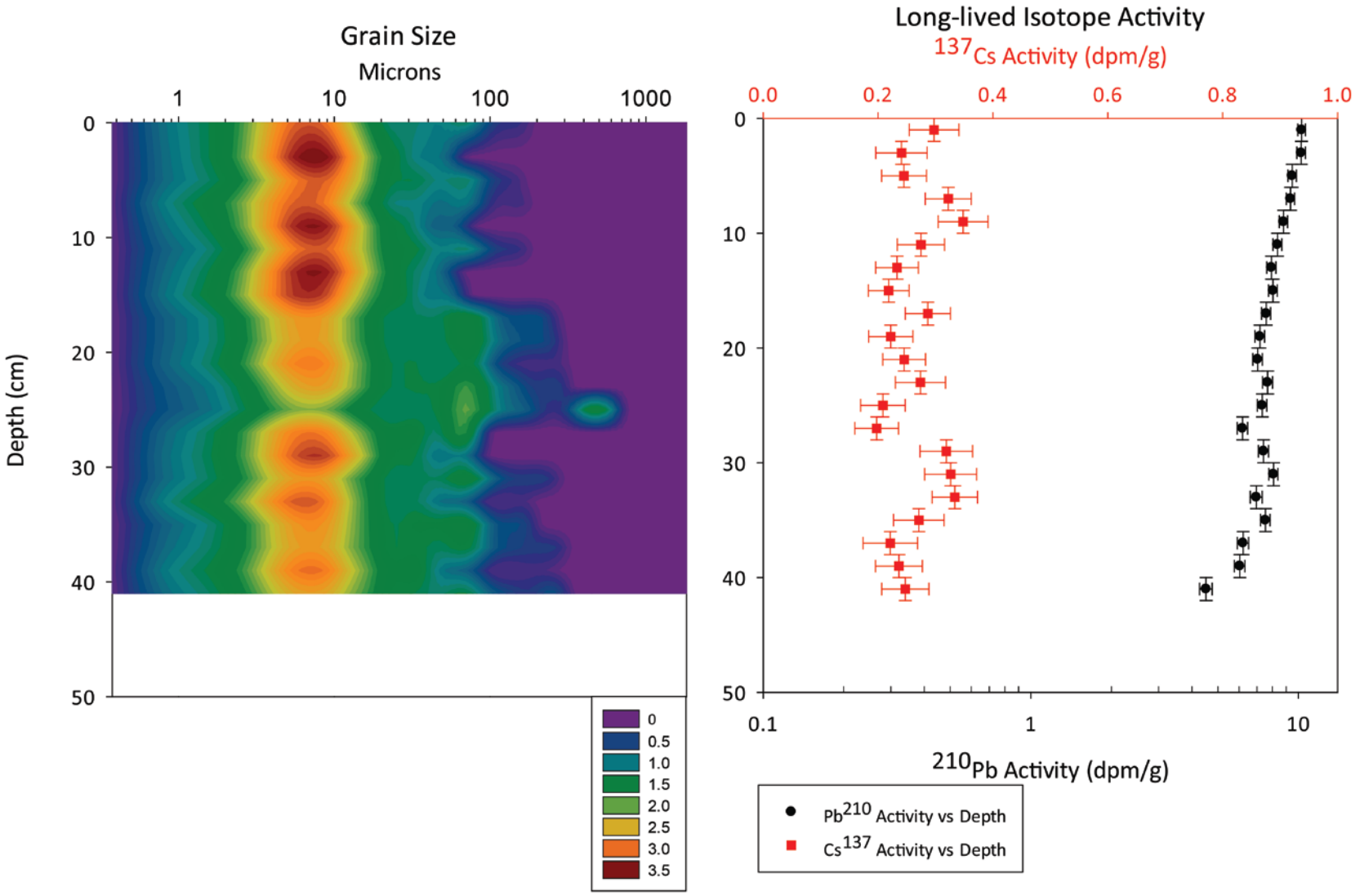

(Appendix I continued)

MRD 14-11

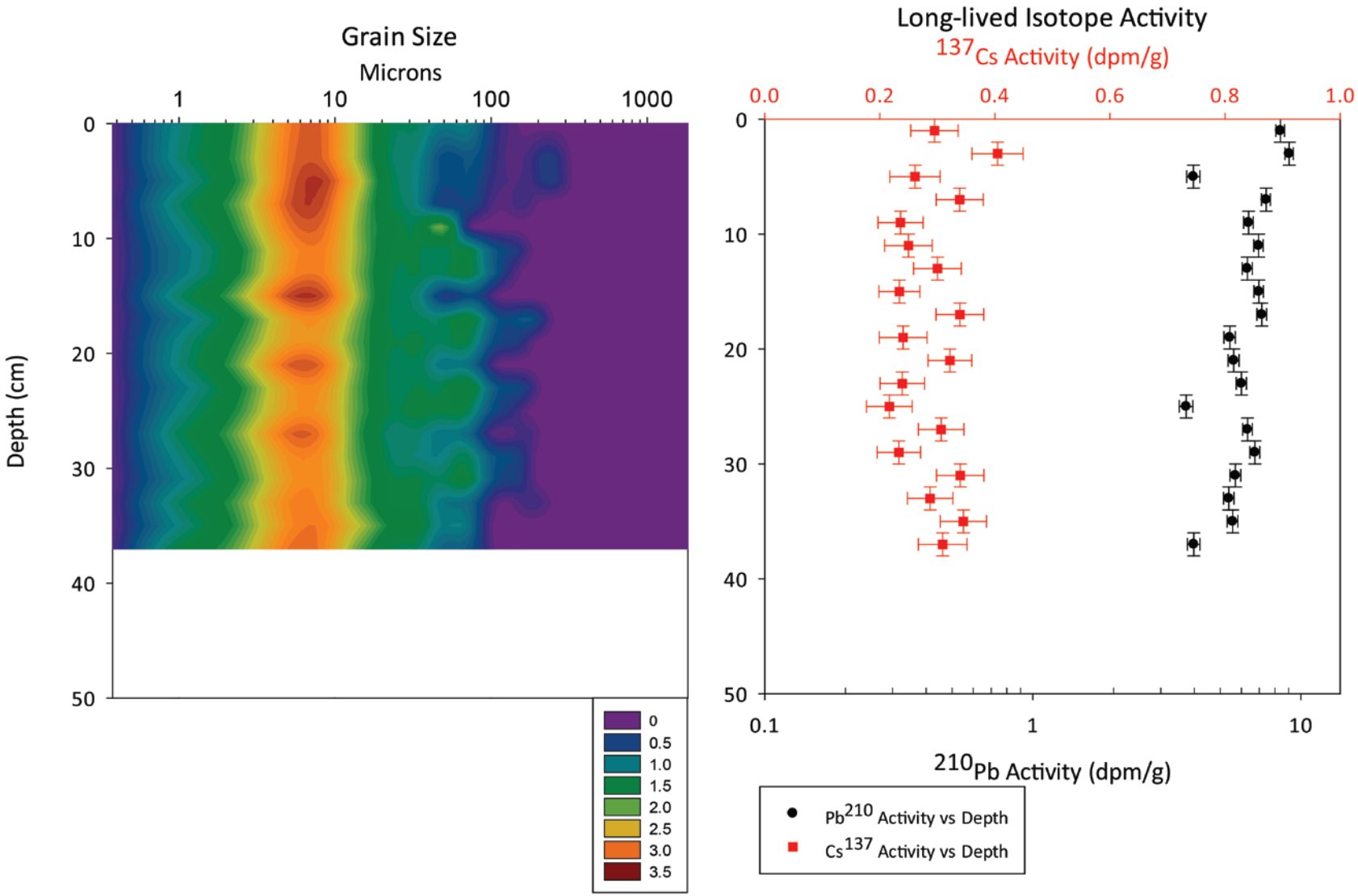

(Appendix I continued)

MRD 14-12

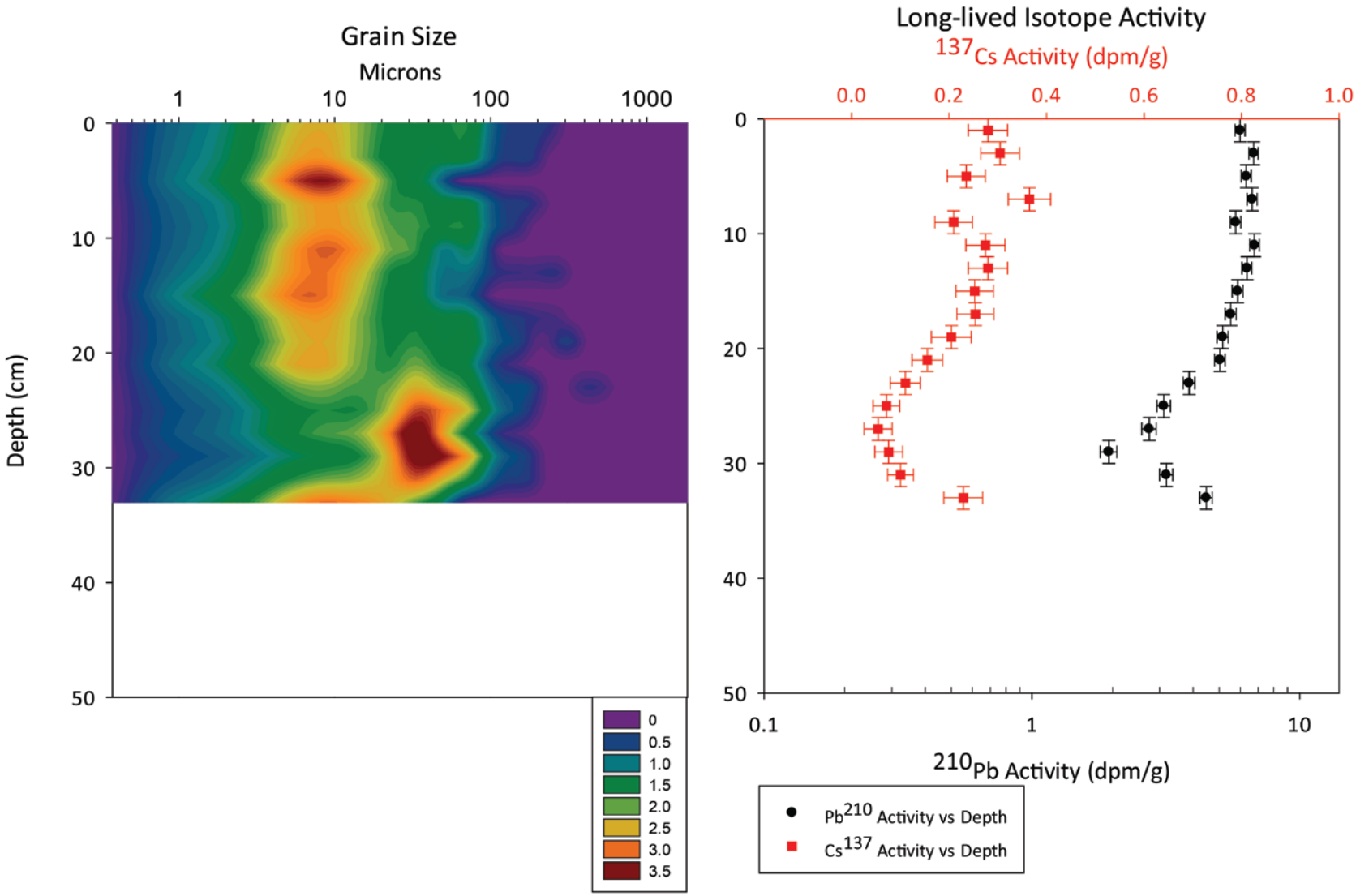

(Appendix I continued)

MRD 14-15

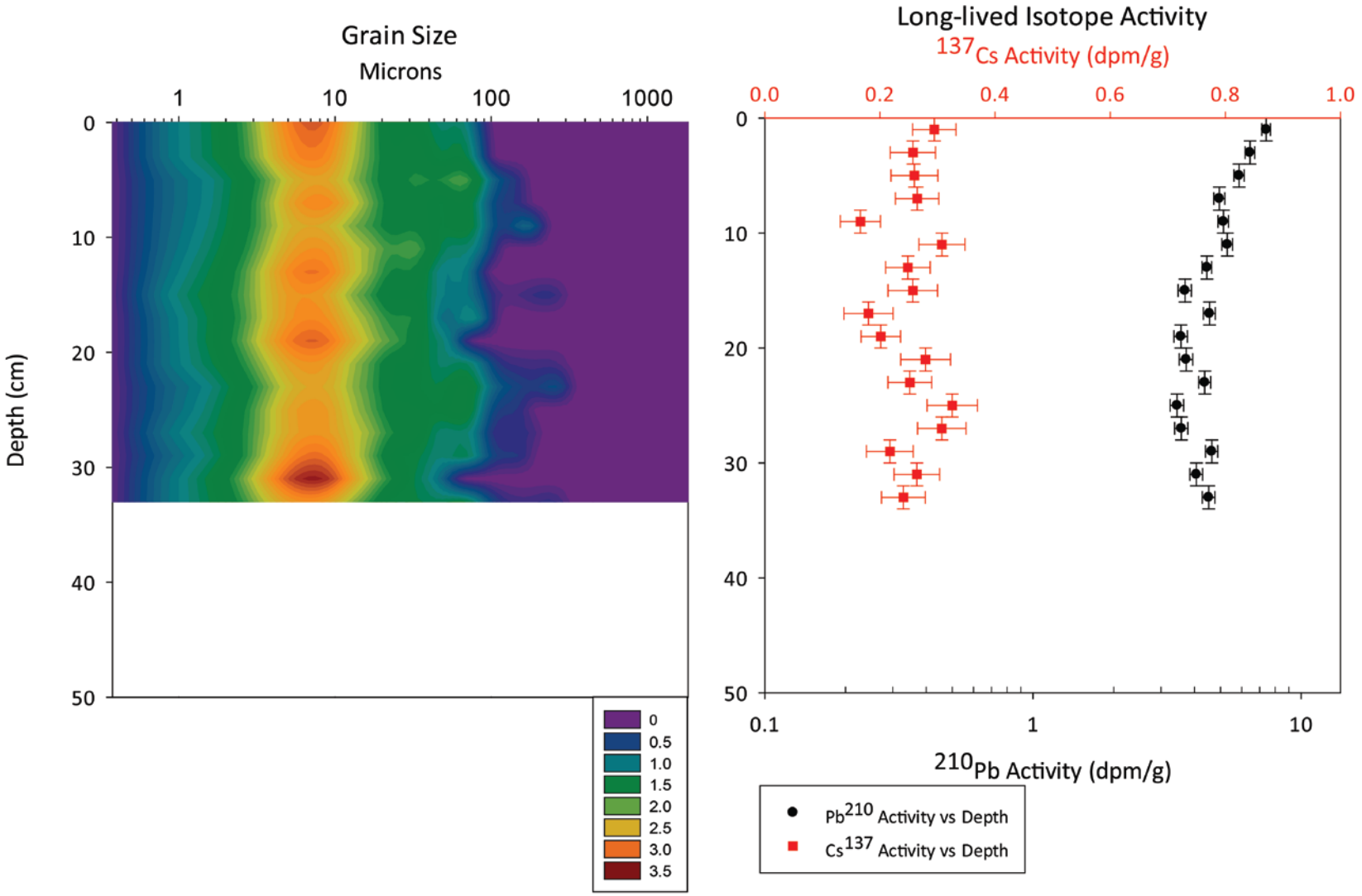

(Appendix I continued)

MRD 14-16

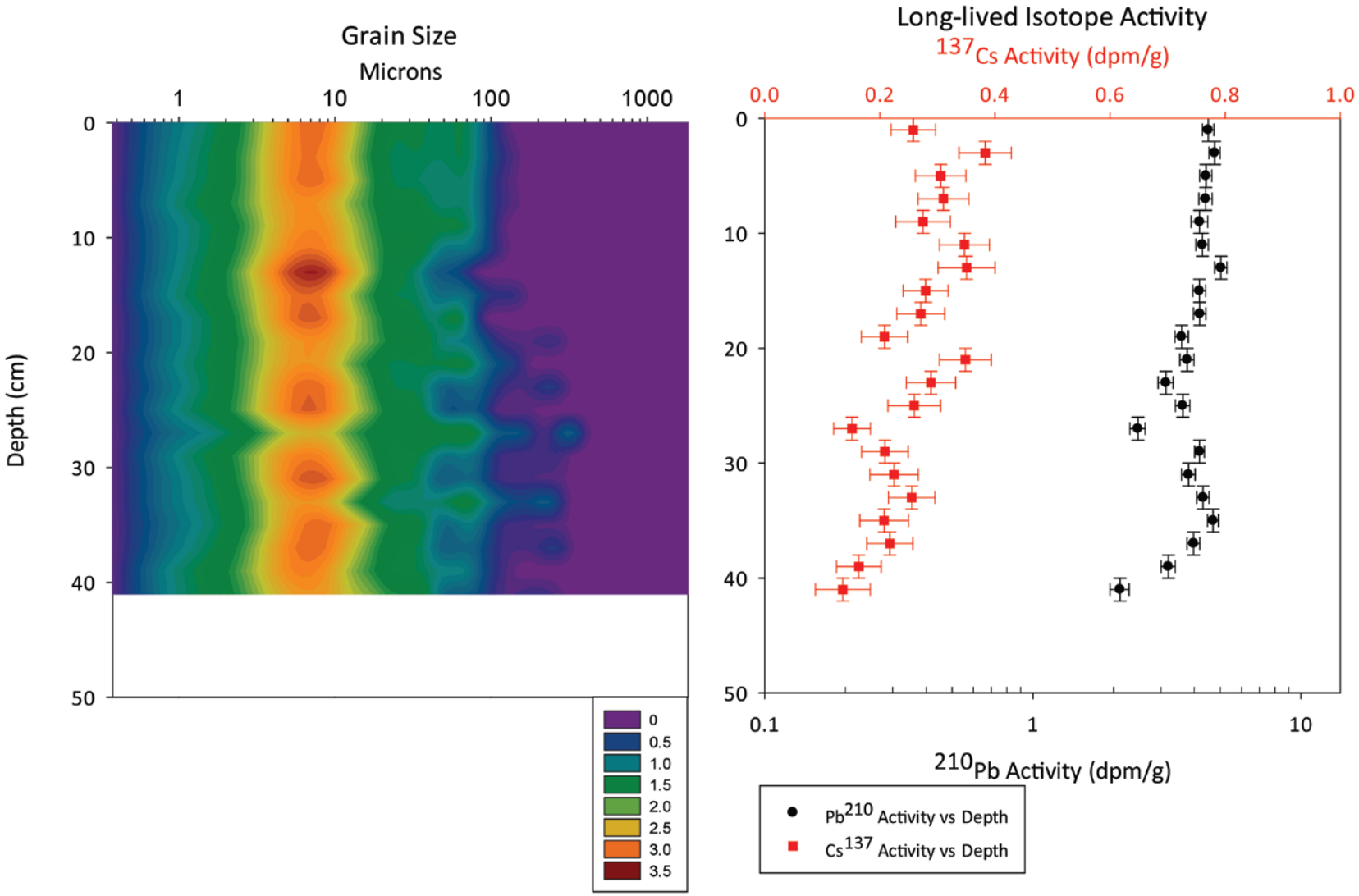

(Appendix I continued)

MRD 14-18

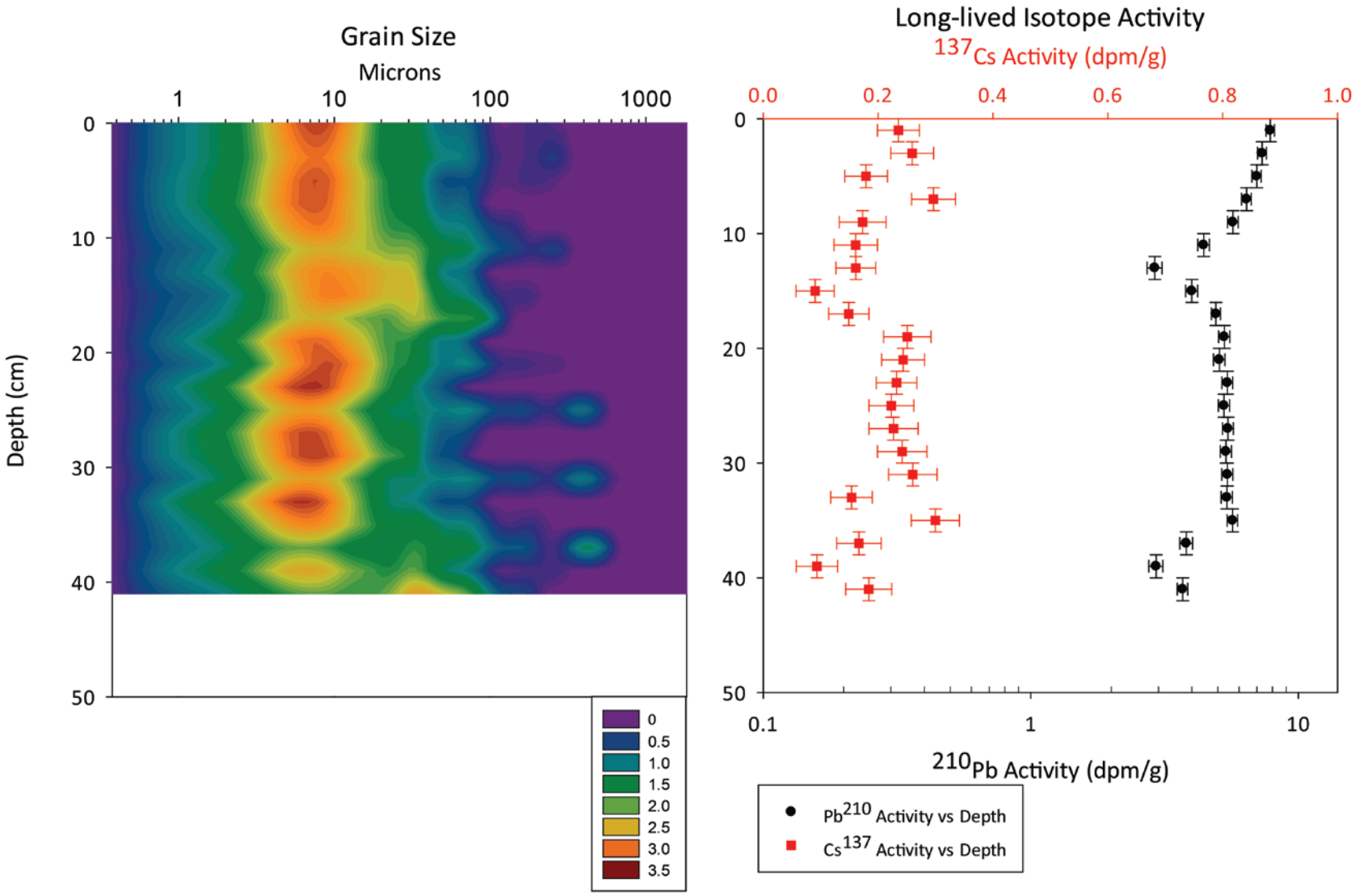

(Appendix I continued)

MRD 14-19

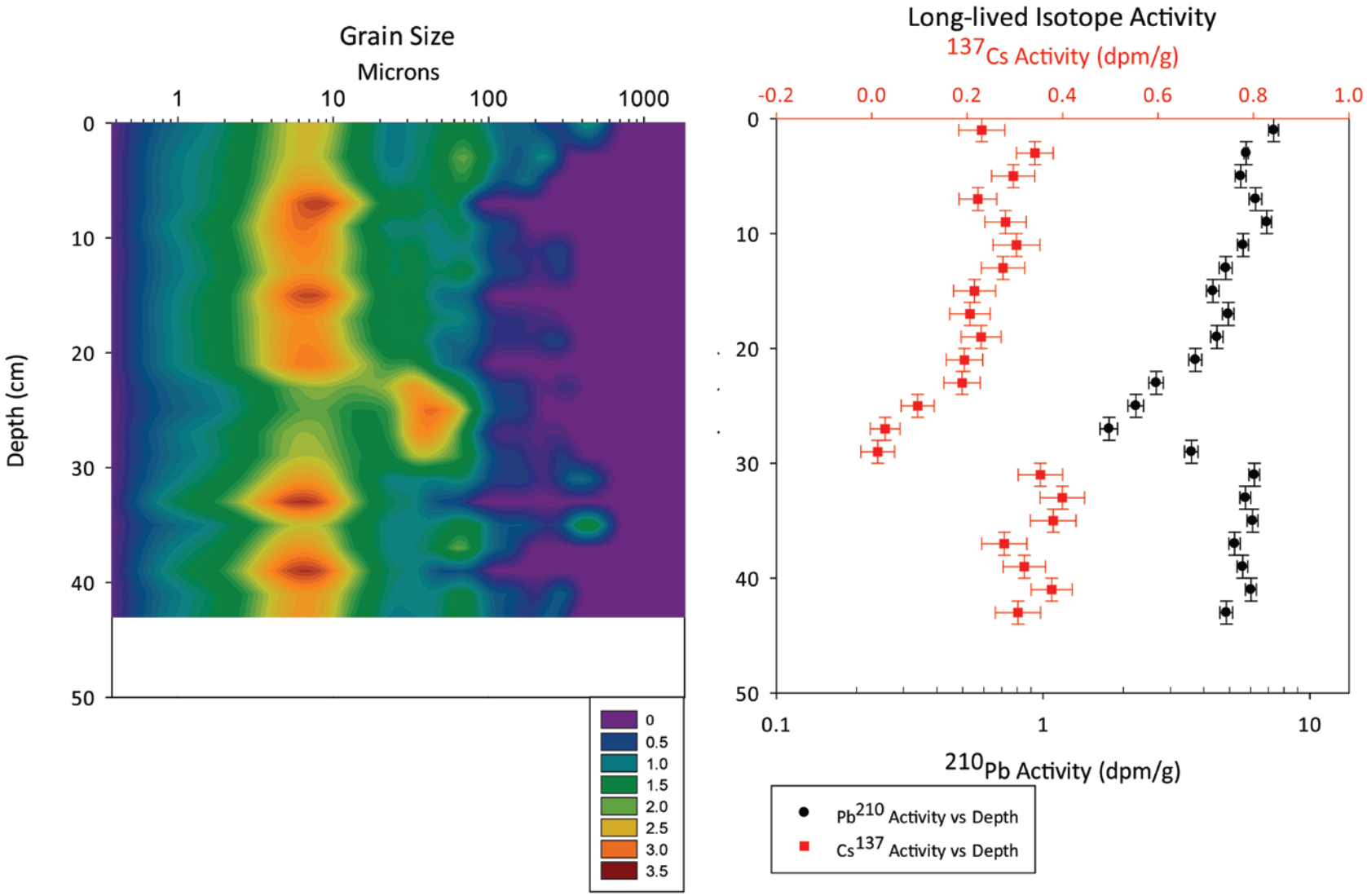

8 Vita

Gregory Paul Keller is a Louisiana native who has always had a love for Louisiana's sedimentary geology, even if he didn't know it when he was younger. He grew up playing on the point bars of the Mississippi River and in the Bonnet Carré spillway. After arriving at LSU in 2009, he realized that studying geology would equip him to work with the landscape he knew and serve the south Louisiana community. After graduation, he plans pursue a career in coastal restoration/research.